Biodegradable Microfluidic Scaffolds for Vascular Tissue Engineering

by

Christopher John Bettinger

S.B. Chemical Engineering
Massachusetts Institute of Technology, 2003

SUBMITTED TO THE DEPARTMENT OF BIOLOGICAL ENGINEERING IN PARTIAL FULFILLMENT OF THE REQUIREMENTS FOR THE DEGREE OF

MASTER OF ENGINEERING IN BIOLOGICAL ENGINEERING
AT THE
MASSACHUSETTS INSTITUTE OF TECHNOLOGY

JUNE 2004

Signature of Author.....

Department of Biological Engineering

Certified by.....

Prof. Robert Langer
Professor of Chemical and Biological Engineering
Thesis Advisor

Accepted by.....

Prof. Douglas A. Lauffenburger
Professor of Chemical and Biological Engineering
Chairman, Graduate Program in Biological Engineering

Biodegradable Microfluidic Scaffolds for Vascular Tissue Engineering

by

Christopher John Bettinger

SUBMITTED TO THE DEPARTMENT OF BIOLOGICAL ENGINEERING IN PARTIAL FULFILLMENT OF THE REQUIREMENTS FOR THE DEGREE OF MASTER OF ENGINEERING IN BIOLOGICAL ENGINEERING

Abstract

This work describes the integration of novel microfabrication techniques for vascular tissue engineering applications in the context of a novel biodegradable elastomer. The field of tissue engineering and organ regeneration has been born out of the high demand for organ transplants. However, one of the critical limitations in regeneration of vital organs is the lack of an intrinsic blood supply. This work expands on the development of microfluidic scaffolds for vascular tissue engineering applications by employing microfabrication techniques. Unlike previous efforts, this work focuses on fabricating this scaffolds from poly(glycerol-sebacate) (PGS), a novel biodegradable elastomer with superior mechanical properties. The transport properties of oxygen and carbon dioxide in PGS were measured through a series of time-lag diffusion experiments. The results of these measurements were used to calculate a characteristic length scale for oxygen diffusion limits in PGS scaffolds. Microfluidic scaffolds were then produced using fabrication techniques specific for PGS. Initial efforts have resulted in solid PGS-based scaffolds with biomimetic fluid flow and capillary channels on the order of 10 microns in width. These scaffolds have also been seeded with endothelial cells and perfused continuously in culture for up to 14 days resulting in partially confluent channels. More complex fabrication techniques were also demonstrated. A novel electrodeposition technique was used in the fabrication of biomimetic microfluidic masters. Thin-walled devices were also synthesized to accommodate the relatively low gas permeability of PGS.

Thesis Advisor: Professor Robert Langer
Title: Professor of Chemical and Biological Engineering

Acknowledgements

June 2004

This thesis was funded by the Charles Stark Draper Laboratory IR&D Project No. 2007.

First and foremost, I would like to thank my family for their motivation and continued support in pursuing my personal goals. This thesis would not have been possible without the love and encouragement of Teresa Tao who has always been my guiding light. I would also like to thank Chris, Buddy, Roger, Aaron and Dickey for their continued creative inspirations during the development of my thesis work. I would like to thank the Departments of Chemical Engineering and Biological Engineering at MIT for providing extraordinary educational opportunities in the classroom as well as in the laboratory, leaving me well prepared to pursue a career in bioengineering research. Specifically, I am grateful for the opportunity to work in the Langer Lab and have Prof. Robert Langer as my thesis supervisor. His creativity, vision, and dedication to science and engineering have been truly inspirational. Special thanks to Jeff Borenstein, Brian Orrick, and the entire Draper Laboratory for their financial support and use of shared facilities.

On a more personal level, I would like to thank the brotherhood of Alpha Mu Chapter of Phi Kappa Sigma whose values and beliefs have equaled the stars in endurance and have helped sculpt me into the man I am today. My membership in this fraternity was instrumental in my undergraduate education as I learned both the power of the beacon of knowledge and the strength of the human spirit. I shall forever carry with me the lessons and love of life that I have gained by living with these fine gentlemen.

TABLE OF CONTENTS

LIST OF FIGURES

LIST OF TABLES

Chapter 1: An Introduction to Tissue Engineering and Organ Regeneration

1.1 The Demand for Engineered Tissues

Tissue loss and organ failure are problems that have plagued health care throughout the world and in the United States. The financial burden of treating these patients have totaled more than $400BB USD annually[1,2]. Standard treatments for organ loss include transplantation, surgical reconstruction, and the incorporation of artificial organs and systems. Although these techniques can save lives, they each carry significant drawbacks, which can negatively affect the patients' quality of life. Reconstruction of lost or damaged tissue can often leave a patient with long-term problems. For example, colon cancer becomes prevalent in patients that undergo a treatment to redirect urine from the bladder to the colon[3]. Transplantation is limited by the amount of organ donors coupled with a rapidly increasing waiting list for organ recipients. In 2003, more than 80,000 patients on the organ recipient waiting list[4](Table 1).

Table 1. 2003 Organ Recipient Waiting List Breakdown by Organ.

Organ	Patients on Waiting List
Kidney	54,651
Liver	17,139
Pancreas	1,422
Kidney-Pancreas	2,420
Intestine	177
Heart	3,742
Heart-Lung	199
Lung	3,873

The problems with current treatments of organ failure and tissue loss have prompted the creation of the tissue engineering. The field of tissue engineering, referred today as regenerative medicine, is an interdisciplinary effort that combines the disciplines of medicine, engineering, and science in

growing, repairing, and improving tissue structure and function. There are three basic strategies that have been studied to create new tissue[5].

1. **Isolated cells and cell substitutes.** This treatment allows for an infusion of specific cells into the patient without the complications of surgery. Although the cells may be manipulated prior to injection, the possibility of loss of cell function and immunological response are imminent.
2. **Tissue growth factors.** High, localized concentrations of signaling molecules could lead to organ regeneration. Success with this approach hinges not only upon the ability to produce massive quantities of these biomolecules, but also targeted delivery. Another strategy to utilize tissue growth factors for tissue engineering is the use of gene delivery systems to upregulate the local production of these growth factors.
3. **Cell-matrix interactions with scaffolds.** Matrices constructed out of natural or synthetic materials can induce cell migration, act as immunoisolation barriers, and provide structural support for the cells to grow and proliferate. The ultimate goal is for the cells to grow and eventual replace a biodegradable scaffold. thereby forming tissue that is functionally equivalent to the desired tissue.

These strategies have been pursued in attempts to grow a variety of tissues including nerve, skin, cardiac and bone. More recent efforts have focused on developing strategies to engineer more complex organs such as the pancreas, kidney, and liver. The field of vascular tissue engineering has been born out of the demand for blood vessels of various dimensions for treatment of coronary artery and peripheral vascular diseases, the leading causes of mortality in the United States[6]. A more recent demand for vascular tissue engineering approaches has also matured to support parallel advances in tissue engineering. General tissue engineering strategies have relied on the natural in-growth of local blood vessels within tissue engineering devices to achieve permanent vascularization

after the device has been implanted. Although this technique may be sufficient for simple tissues such as skin, bone, or cartilage, it is not sufficient for highly vascularized organs such as the kidney and liver. Traditional tissue engineering approaches to these problems have focused on the *in vitro* growth of various combinations of endothelial cells and smooth muscle cells in macroscopic constructs using biomaterials such as Dacron[7]. Although these strategies have shown promise, they lack the ability to precisely control the cellular microenvironment. *In vivo* vascular tissue engineering therapies have attempted to induce blood vessel growth and maturation by using a variety of approaches including controlled drug release and gene therapy. Controlling the signaling molecules in the microenvironment is essential for engineering native-like blood vessels in both *in vivo* and *in vitro* approaches.

1.2 Biology and Biochemistry of Blood Vessels

It is tempting to overlook the importance of biochemical signaling pathways and concentrate on biomaterials and other design components when developing tissue-engineering platforms. However, it is of utmost importance to understand the relevant biochemical and signaling pathways that are present in the growth of tissues. More specifically, the proliferation and maturation of blood vessels is a critical component in vascular tissue engineering.

1.2.1 Relevant Biomolecular Signaling and Pathways in Blood Vessel Proliferation and Maturation

The utilization of tissue growth factors is a promising approach for tissue engineering blood vessels. However, recent studies have determined that the growth and maturation of blood vessels is a complex biological process that involves numerous cell types and uses numerous signaling pathways (Figure 1). Spatio-temporal coordination between the cells and corresponding arrays of various

signals is critical for angiogenesis. Therefore, it is important to understand the details of the relevant biological signaling involved in angiogenesis and maturation first before the development of potential therapies for vascular tissue engineering using tissue growth factors. In *in vivo* systems, endothelial cells (ECs) migrate and proliferate in the presence of large amounts of vascular endothelial growth factor (VEGF) to form new blood vessels in the presence of arteriogenetic environments, which will be discussed later[8]. These nascent blood vessels consist of a monolayer of ECs in a tubular conformation with individual cobblestone cell morphology. The first step towards maturation is the recruitment of surrounding mural cells. This process is regulated by four processes; 1) platelet-derived endothelial growth factor (PDGF); 2) sphinogosine-1-phosphate-1 (S1P1)—endothelial differentiation sphingolipid G-protein-coupled receptor-1 (EDG1); 3) A tyrosine kinase receptor (Tie-2) and angiopoitein (Ang-1); 4) transforming growth factor (TGF-B).

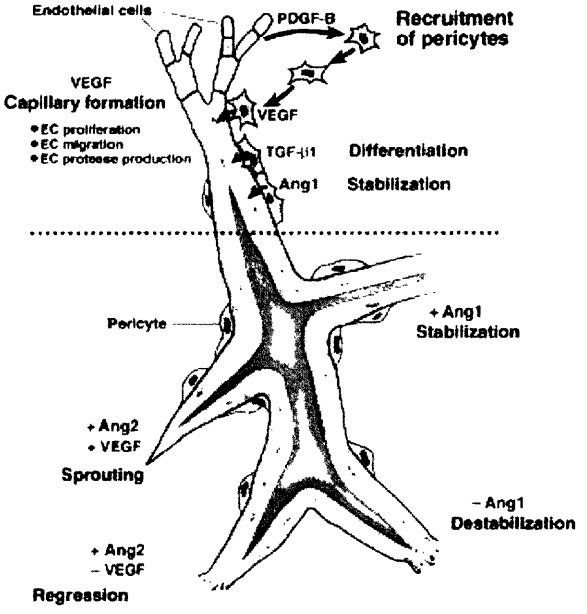

Figure 1. Overview of Regulation of Vessel Assembly. After ECs self-assemble into monolayer tubules, they begin recruiting pericytes using PDGF-B. This leads to maturation of the nascent blood vessels. The additional presence of Ang1 leads to further stabilization while Ang2 in combination with VEGF induces sprouting.

PDGF. PDGF is a molecule that is secreted by many cell types including ECs. However, the importance of PDGF during blood vessel maturation has been supported through evidence of *Pdgfb* knockout mice, which encounter embryonic lethality[9]. These mice exhibit aberrant vessel remodeling along with the absence of pericytes of the microvasculature[10]. This observation illustrates the critical role that PDGF plays in recruiting local pericytes and eventual blood vessel maturation. Phenotypical similarities between *Pdgfb* and *Edg1* knockout mice also suggest a similar importance of the EDG1 receptor during vessel development.

Tie1/2 Ligands and Ang1/2 Receptors. The role of Tie1 and Tie2 and their receptors, Ang1 and Ang2 are also essential for maturation. Ang1 serves to stabilize nascent blood vessels, although the mechanism is still unclear. Alternatively, the effect of Ang2 appears to be situational. Namely, if local concentrations of VEGF are increased, Ang2 appears to induce arteriogenesis. However, if levels of VEGF are relatively low, then Ang2 serves to destabilize blood vessels[11]. This hypothesis was tested in 3-D spheroidal co-culture assay. Direct contact between ECs and Ang1-expressing mesenchymal cells leads to a decreased responsiveness to VEGF whereas the presence of Ang2 and VEGF results in angiogenesis. Further evidence of this effect has been shown in the microvascularization of rat testes[12]. Local injection of Ang2 in the testis increases endothelial cell proliferation as well as the volume of the interstitial space thereby supporting the proposed hypothesis.

TGF Pathways. Once the EC wall successfully recruits the pericytes, the ECs begin producing TGF-B, which has been observed to interact with a number of signaling pathways between cells. In the context of blood vessel maturation processes, TGF-B1 promotes maturation by stimulating

extra-cellular matrix (ECM) production by differentiating mesenchymal cells to mural cells. TGF-B also acts on two complementary downstream pathways named TGF-B-ALK1 and TGF-B-ALK5 respectively. The ALK1 pathway serves to induce proliferation and migration of fibroblasts to the EC tube via the Id1 protein. The ALK5 pathway induces the plasminogen activator inhibitor (PAI)1 in ECs, which promotes vessel maturation. Therefore, the relative strength of signaling present in the ALK1 and ALK5 pathways leads to cell migration and proliferation or vessel maturation.

Remodeling of Mature Vessels. The basement membrane and surrounding ECM provide additional cues for the fate of blood vessels. Proteins that compose the ECM surrounding mature blood vessels function as storage sites for signaling molecules that regulate the proliferation, survival, and migration of the vessels. The degradation of this ECM by various proteases releases angiogenic molecules such as VEGF and fibroblast growth factor (FGF). Additionally, these proteases also serve to release anti-angiogenic molecules by cleaving various ECM molecules or even the proteins themselves. For example, numerous approaches indicate that fibronectin, collagen, and their respective receptors are proangiogenic. Consequently, these space and time-dependent concentration profiles of the various signaling molecules regulate the overall balance of proliferation and regression of ECs and mural cells alike. However, further elucidation of the complex, multifactorial cell-matrix interactions must be attained before this information can be effectively applied in tissue engineering applications.

The Effect of Surrounding Tissues on Mature Blood Vessels. The thought that microvasculature is a system of dormant, inactive tissues has been abolished. Instead, it is now thought that blood vessels, including ECs, are able to communicate with surrounding tissues, which

in turn affect their phenotypic disposition. In other words, blood vessels take on the attributes of their surrounding microenvironment while also maintaining some degree of variability in their eventual cell fate[13]. The surrounding tissues regulate the vessel architecture by means of VEGF. Locally secreted VEGF signals induce various types of EC behavior. In addition to the ubiquitous VEGF-A system, there has also been a recent discovery of tissue-specific vascular endothelial growth factors. For example, endocrine gland VEGF (EG-VEGF) is functionally similar, yet structurally distinct from its VEGF-A counterpart. Furthermore, EG-VEGF does not affect ECs from the aorta or umbilical vein, which leads to the hypothesis that such a molecule only functions in a specific organ. Therefore, tissue-specific VEGF may complement the more ubiquitous VEGF-A molecules in regulating EC growth and maturation in blood vessels.

1.2.2 Role of Microenvrionment in Blood Vessel Maturation

The previous section outlined the relevant biological pathways that are critical to the fate of blood vessels. Another critical element of blood vessel engineering is the precise control of the microenvironment of the cells. In addition to the chemical environment, blood vessel maturation pathways are both directly and indirectly affected through physical parameters such as oxygen concentration, pH, hydrostatic pressure and mechanical shear stress. Carefully adjusting these parameters to create an angiogenic microenvironment could help advance tissue engineering of mature blood vessels in both *in vivo* and *in vitro* environments.

Mechanical Microenvironment – Shear Stress. Two types of shear stresses that ECs of blood vessels are commonly exposed to are laminar (LSS) and distributed (DSS). LSS, which is associated with flow parallel to cell layers, can be further classified as either acute or chronic (Figure 2). LSS has also been shown to induce a variety of endothelial activation genes, which leads to a general

predisposition to arteriogenesis while DSS tends to suppress endothelial activation genes, which results in quiescence combined with a general anti-apoptotic and anti-inflammatory state. There have been various *in vivo* studies which suggest that arteriogenesis can occur when the mechanical environment both inside and outside the cell is changing[14]. Subsequent studies have supported this model by suggesting that increases in shear rate function as the primary signal for arteriogenesis[15]. Periodic shear stress has also been shown to both stimulate endothelial cell migration in non-confluent structures as well as assist in mechanisms of blood vessel maintenance. DSS, which is generally characterized as perpendicular flow relative to a cell monolayer, results in a number of cell activities, which eventually lead to atherogenesis in both acute and chronic timescales.

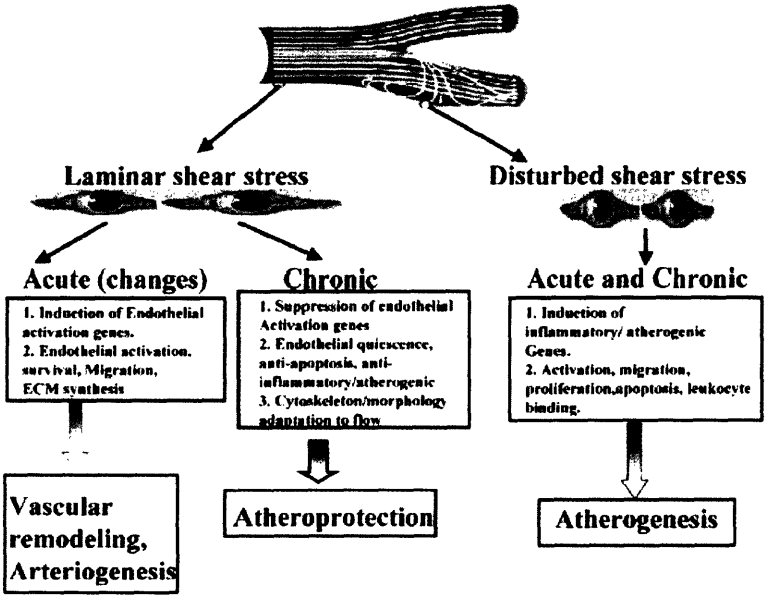

Figure 2. Response of ECs to Various Shear Stress Patterns. The type of shear stress ECs experience in part, determines the fate of the cells. This information is critical in either the design of a biomimetic system for EC culture or as an *in vivo* parameter for inducing vascular therapies.

Effect of Shear Stress on Endothelial Gene Regulation. The cellular responses of ECs are extremely dependent upon the shear stress pattern. Varieties of non-laminar shear stress have a full

range of effects on EC gene expression. For example, pulsatile shear stress results in increased expression of PDGF-A[16]. In mouse models, oscillatory shear stress was found to increase the expression of vascular cell adhesion molecule-1 (VCAM-1), which is critical for forming tight junctions between adjacent ECs[17]. For example, ECs at regions of flow circulation such as bifurcations and curvatures also have expressed elevated levels of VCAM-1. Furthermore, a distributed non-LSS has also been shown to regulate gene expression in blood vessel ECs. Studies have shown that ECs in a non-LSS environment rapidly undergo cycles of proliferation, migration, and death, which suggest an elevated anti-quiescence among the cell population. These results suggest that a non-LSS environment leads to a more active state for ECs relative to a LSS environment.

Incorporating Shear Stress Factors into System Design. In general, studies have shown that periodic shear stresses lead to increased proliferation, migration, and adhesion in both *in vivo* and *in vitro* systems. Perfusion systems for vascular engineering applications are the obvious target for manipulation of fluid mechanical microenvironments for increased arteriogenesis *in vitro*. There are a number of strategies that can be used to achieve periodic shear stress. One possible method is to install a two-way valve, which is attached in-line with a constant driving force such as a syringe pump or a peristaltic pump with an in-line dampening chamber. When the valve is closed, pressure is building up within the volume in the line behind it. Upon triggering the opening of the valve with a timing circuit or other control system , the media is released in a short quick burst followed by a rapid decay in pressure. This technique is a simple addition that can be added in-line with pre-existing perfusion systems that provide constant LSS. Another method of establishing a dynamic shear stress environment is to use a peristaltic pump in the perfusion system. The inherent pumping mechanism results in an approximately sinusoidal waveform. Although the resulting waveform is by

no means biomimetic, a dynamic shear stress is achieved nonetheless. One potential drawback of such pumps is the lack of amplitude in the pressure waveform. If the growth of a single blood vessel with an inner diameter of > 2 mm is desired, then one could use a novel pulsatile system that attempts to mimic physiological waveforms[18]. By using a network of valves and manifolds, unique systems have been developed especially for vascular tissue engineering applications.

Channel geometries and flow rates must also be considered due to their direct affect on the mechanical microenvironment. In addition to shear stress, there are numerous other parameters that can have a dramatic impact on ECs in vitro such as linear velocity, shear rate, and vorticity. Finite-element simulation programs can play a crucial role in predicting the mechanical microenvironment in biomimetic geometries with parameterized volumetric flow rates (Figure 3). Correlating the results of the simulation with experimental data can lead to additional characterization of the effect of fluid mechanics on EC attachment, proliferation and migration.

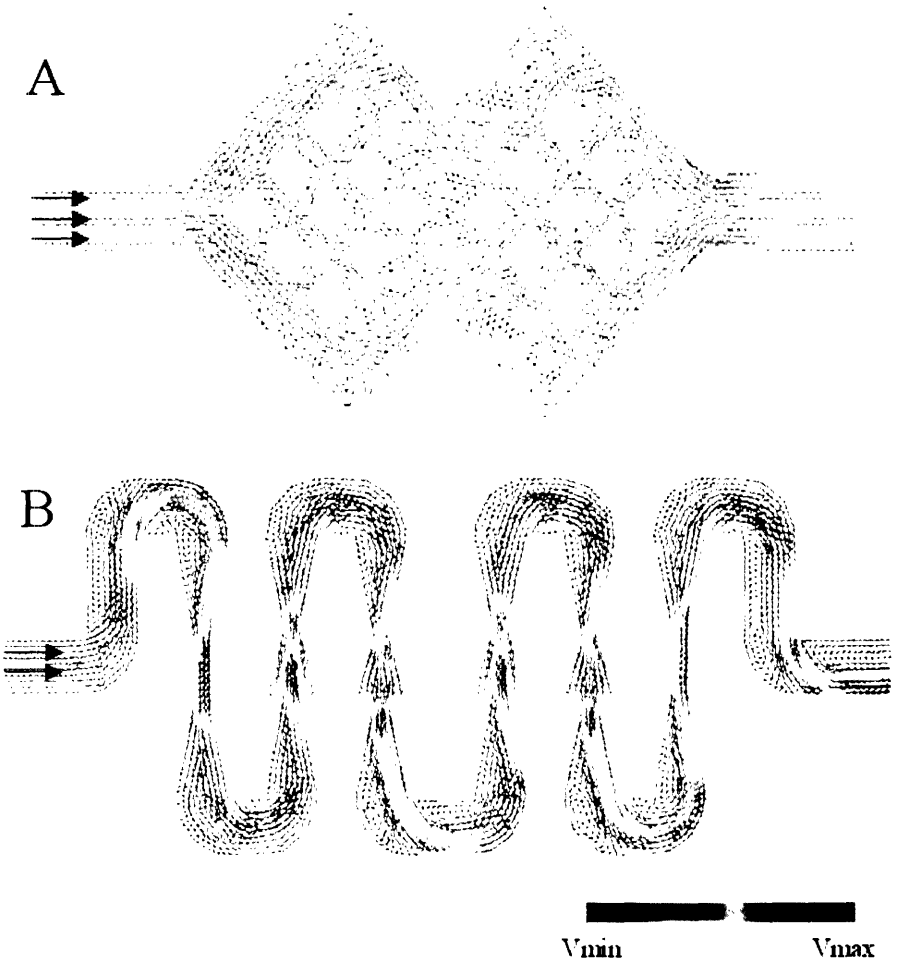

Figure 3. Simulated Velocity Vector Fields in Microfluidic Devices. A) This figure illustrates the relative velocities in a simulated capillary bed design for applications in microreactors. B) A microfluidic device pattern that can be used as a potential diagnotistic tool for studying the effect of characteristic flow fields on ECs. This specific device would be used to study the effects of both gradual and rapid expansions and contractions. Additional simulations can also examine critical fluid mechanical properties such as shear stress, vorticity, and Reynolds number. These simulations were performed using Fluent 6.0 finite element simulation package in combination with Gambit 2.0 mesh constructor and plotted using TecPlot[19].

Metabolic Microenvironment. Although the mechanism for oxygen concentration detection along with the transmission of this information to regulatory pathways remains unknown, we do know that oxygen homeostasis is dependent upon hypoxia-inducible factor-1 (HIF-1), a

transcriptional activator that functions as the master regulatory molecule [20]. There are twelve known target genes of HIF-1, but its transcriptional activity is thought to regulate hundreds of genes including those related to angiogenesis. In addition to oxygen concentration, HIF-1 can be activated via redox signals or kinase cascades by a number of molecules including nitric oxide, cytokines, and other growth factors. Although the current understanding of these signaling mechanisms remains limited, current theories speculate that a gene activation response to hypoxia is not a simple linear signaling pathway, but a complex, multifactorial web of signals and receptors. Nonetheless, expanded knowledge into the mechanism of hypoxia-induced angiogenesis would prove beneficial to current efforts in blood vessel engineering. For example, cytokines and growth factors involved in HIF-1 activation could be supplied directly to a blood vessel culture in order to stimulate sprouting and proliferation. Local variations in the metabolic cellular microenvironment are able to produce angiogenic and anti-angiogenic effects. In addition to hypoxia, glucose deprivation and acidic pH values are known to induce angiogenesis in a wide range of tumor cell lines[21]. Both *in vivo* and *in vitro* experiments have confirmed that decreasing the pH leads to upregulation of VEGF via the Ras and mitogen-activated protein kinase (MAPK) pathways and the subsequent signaling molecule AP-1.

1.3 Vascular Tissue Engineering

1.3.1 Delivery of Tissue Growth Factors

As previously mentioned, the precise spatio-temporal concentration of specific growth factors is critical to growth and maturation of blood vessels. The rapidly advancing fields of biomaterials and biopolymers have made controlled release of therapeutic agents a reality. Gene therapy techniques can also be applied to facilitate desirable *in vivo* responses.

Feedback Response Delivery Systems. Most of the previously developed polymer-based drug delivery systems are used in static conditions where the drug is released at a predetermined rate. Although changing the polymer formulation can alter the release pattern, these devices are not "smart" in the sense that they cannot respond to peripheral stimuli. However, a recent improvement upon this class of systems allows for the modulation of release kinetics by external mechanical signals. One alginate hydrogel system can upregulate the release of VEGF in response to mechanical stimuli[22]. The properties of the material in this system are critical. Namely, the material must be able to withstand repeated deformation and also permit the reversible binding of VEGF protein. When programmed to release VEGF, this engineered ECM has been shown to increase both the blood vessel number and blood vessel density in SCID mouse models in response to mechanical stimulation. These systems could have a dramatic impact on both *in vivo* vascular therapies and *in vitro* vascular tissue engineering applications. The biocompatibility and biodegradability of the hydrogel polymer serves to increase the number of applications of this system.

Temporal Control of Delivery of Multiple Signaling Molecules. Another unique type of drug delivery system accommodates the necessary time-dependent exposure of nascent blood vessels to various types of growth factors. This can be accomplished by using a heterogeneous polymer system that can control the release of multiple cytokines (Figure 4). Furthermore, the release of these signaling molecules can occur at different, predetermined rates[23]. The variable kinetics of the system is achieved by imbedding polymer microspheres within a larger polymer scaffold. This system can be used to deliver VEGF and PDGF to a specific location in temporal sequence. The VEGF-infused scaffold slowly degrades by hydrolysis, releasing the VEGF molecule at a controlled rate. When this polymer system has degraded sufficiently, the PDGF-containing microspheres are exposed. The subsequent rapid hydrolysis of the microspheres then releases PDGF-B in a timely

manner. *In vivo* studies of this technology have resulted in a high degree of neovascularization and maturation.

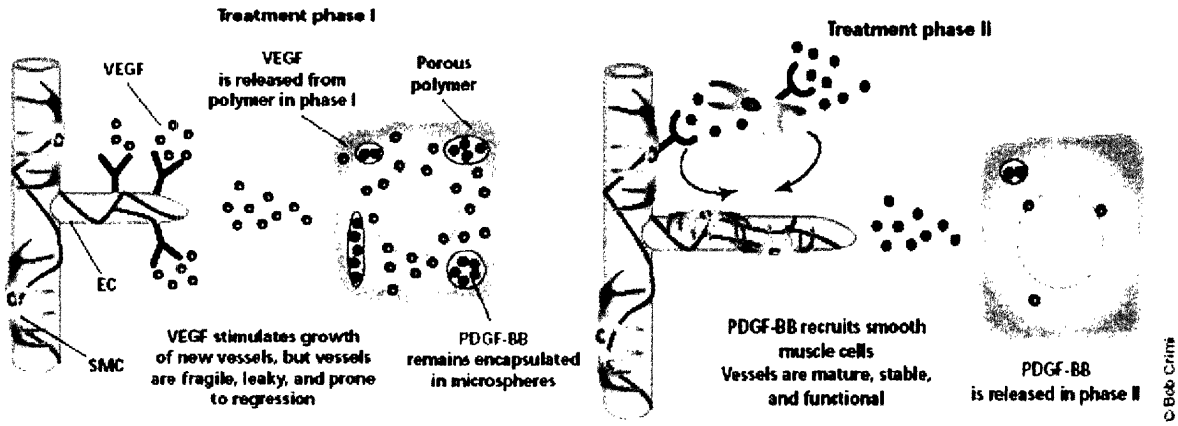

Figure 4. Heterogenous Polymer Controlled Drug Release System[23]. The controlled release kinetics of two angiogenic factors aids in the engineering of mature vessels. Intially, VEGF is released which induces EC proliferation and angiogenesis. In the second phase, PDGF-BB is released to recruit SMCs, which are necessary for blood vessel maturation.

Gene Transfer for Use in Therapeutic Vascular Growth. Gene therapy provides a possible alternative for *in vivo* vascular growth. Therapeutic vascular growth using gene transfer uses the standard strategies and exhibits near-identical characteristics and benefits as traditional gene therapy procedures. Adenoviruses are the standard vector for gene delivery and insertion. However, gene therapy for vascular growth aims to produce increased amount of cytokines and chemokines such as various types of VEGF, placental growth factor (PLGF), fibroblast growth factor (FGF), and angiopoiteins[24]. Therapeutic vascular growth has also focused on both the constitutive and inducible expression of other factors involved in vascular growth including the multifunctional protein, hepatocyte growth factor (HGF). Another potential strategy is to induce cellular genes that, in turn, stimulate angiogenesis via a number of signal transduction proteins or transcription factors. This goal can be accomplished through the targeted insertion of genes that code for transcription factors such as nitric oxide synthetase (eNOS), inducible NOS (iNOS) and hypoxia-induced

transcription factor (HIF-1). One potential benefit of using gene transfection is the selectivity towards inducing angio- and ateriogenesis, but not lymphangiogenesis. As with most gene therapy applications, there are significant problems in gene transfer efficiency in large mammals. Nonetheless, gene therapy for vascular therapies has been able to overcome other traditional barriers of treating monogenetic disorders and, as a result, has shown positive results in some animal models. For example, preclinical wound healing models have shown the enlargement and proliferation of the capillaries when treated with adenovirus-mediated delivery of VEGF for more than 4 weeks. If the treatment were stopped before this critical time period, the vessels would regress.

Blood Vessels Derived From Stem Cells. Traditional tissue engineering strategies have focused on utilizing differentiated cell types for regeneration of specific organs and tissues. For example, chondracytes are used for cartilage and hepatocytes are used for liver engineering applications, respectively. However, the recent developments of human embryonic stem (hES) cells have opened the door for new, exciting tissue engineering strategies. hES cells have the potential to differentiate into various types of cells. Therefore, they may be a useful source of cells for tissue engineering applications. A procedure that isolated hES cells using an antibody for PECAM1 was recently reported[25]. *In vitro* techniques have induced the newly differentiated stem cells to produce conformal geometries as well as cellular markers that similar to ECs. Stem cells have also differentiated controllably to produce blood-containing vascular microstructures *in vivo*. This discovery may prove to be effective in engineering new blood vessels and treatment of regional ischemia. However, this advancement may also set the groundwork for engineering mature blood vessels by selectively differentiating hES cells thereby creating a co-culture environment. By precisely controlling the delivery concentration of cytokines and chemokines in the cellular microenvironment using previously detailed methods, a single population of ES cells could selectively differentiate into both

EC cells and mesenchymal cells, which are necessary for blood vessel maturation, in close proximity to each other.

1.3.2 Cell-Matrix Interactions for Vascular Tissue Engineering

Controlling cell-matrix interactions with synthetic biomaterials can induce desirable *in vitro* cellular responses. This approach exhibits often-significant advantages over the *in vivo* delivery of growth factors and cytokines. For example, more recent work with stem cells has focused on the formation and organization of hES cells into more complex three-dimensional vessel networks using porous biodegradable scaffolds[26]. These scaffolds, which were fabricated out of poly(L-lactic-co-glycolic acid) (PLGA) and poly(L-lactic acid) (PLA), provide physical cues for stem cell differentiation while also allowing sufficient void volume for proliferation and remodeling activities in cells. After seeding the polymer constructs with actively differentiating hES cells, they were cultured in the presence of various growth factors for several weeks. Depending on the growth factor, the cells exhibited properties similar to various developing tissues types including neuronal, cartilage, and liver. Furthermore, the hES cells were also shown to differentiate and organize into 3D vascular networks, which was supported by successful CD34 staining. When the cell-seeded construct was implanted into SCID mice, not only did the cells remain viable, but they were recruited by the host vascular system as they continued the *in vitro* progression and differentiation.

General Strategies for *in vitro* Vascular Tissue Engineering. Inducing the growth and maturation of blood vessels can be accomplished *in vivo* as a direct therapeutic approach or *in vitro* using both traditional and non-traditional tissue-engineering methods. Presumably, the goal of *in vitro* tissue engineering is to successfully culture vessels for eventual implantation into a host. There are wide ranges of general strategies that can be used for creating viable microvasculature. One traditional approach is to culture cells on a biodegradable polymeric scaffold. After two months of

perfusion, the newly grown tissue can be implanted into the host. This strategy has proven to be successful in the growth of functional arteries[27]. In this system, ECs and smooth muscle cells (SMCs) were cultured on poly-glycolic acid (PGA) polymers in a biomimetic bioreactor under both static and pulsatile flow conditions. After 8 weeks of perfusion, the gross appearance of the cultured vessels was identical to that of native vessels. The wall thickness for vessels grown under pulsatile flow conditions was also significantly larger than those grown under static conditions. This result illustrates the importance of creating a biomimetic mechanical microenvironment for *in vitro* culture of vessels. These studies have demonstrated the potential of co-culturing SMCs and ECs directly rather than inciting the recruitment of SMCs by the ECs. Therefore, these vessels may not exhibit the ideal characteristics of a native, mature blood vessel.

1.4 Applications of Microfluidic Devices for Tissue Engineering

Tissue engineering bioreactor technology is sufficient for culturing single blood vessels with diameters on the order of 1 mm or greater. These systems lack the spatial resolution and features for culturing complex networks of blood vessels. However, the rapidly growing field of BioMEMS enables the creation of microfluidic systems that can be modified to culture endothelial cells. Silicon etching has been used recently in the fabrication of microfluidic bioreactors for engineering tissues of various types[28]. Endothelial cells were cultured in silicon microchannels that were capped with pyrex glass (Figure 5). Viable cell monolayers were successfully removed from the microreactor and implanted into rat omentum. This process was also demonstrated in the culture of hepatocytes[28]. Silicon etching is also applicable to the fabrication of microfluidic masters for use in replica molding. Poly(di-methyl siloxane) (PDMS) is an inexpensive elastomer that is often used in the fabrication of microfluidic devices for a variety of applications including tissue engineering[29]. PDMS-based

microfluidic systems have been designed to mimic microvascular structures and flow geometries for use a vascular tissue engineering bioreactor[30]. The microchannels in the device were coated with synthetic ECM peptides to aid in cell adhesion of cells and provide an angiogenic cue. The device is seeded with endothelial cells and perfused in a continuous fluidic circuit. After several weeks in culture, the ECs tend to proliferate and form junctions as the channels become confluent. Microfluidic devices have also been fabricated from PLGA[31]. However, this material is not desirable for a tissue engineering scaffold for reasons outlined later in the text. Nonetheless, the advantages of using such a microfluidic system are immediately obvious. The channel geometries can be constructed in such a way to mimic physiological geometries and length scales of blood vessels. Consequently, the fluid mechanic microenvironment can be controlled with great precision. Manipulating geometries on the sub-micron can lead to new abilities in guiding tissue formation and regeneration by inducing selected cellular responses. This newfound control can be expanded to other types of tissue engineering including the culture of hepatocytes. Complex methods and devices have also been developed more recently using PDMS microfluidic systems. Three-dimensional PDMS microfluidic devices have been fabricated for the perfusion culture of a liver cell model[32]. The high gas permeability of PDMS allowed for high-volume tissue engineering constructs while maintaining sufficient oxygen concentrations. Micropatterning of co-cultures for vascular tissue engineering applications has also been achieved [33]. The deposition of three-dimensional cell layers has been demonstrated in PDMS microfluidic devices. A layer-by-layer approach to microfluidic patterning of heterogeneous cells and matrices can lead to the co-culture of ECs, smooth muscle cells, and fibroblasts. This technique could provide strong angiogenic and maturation cues due to the potential for cross-talk between the different cell types. However, the disadvantages to using silicon or PDMS as a biomaterial platform are obvious. Neither silicon nor

PDMS is biodegradable or exhibit *in vivo* biocompatibility. Therefore, synthesizing and manipulating application specific biomaterials is a necessity for tissue engineering.

Figure 5. Perfusion Culture of ECs in Silicon Micromachined Networks[28].

Engineering mature blood vessels is complex task that requires an interdisciplinary approach. First and foremost, the biochemistry of the tissues must be continue to be elucidated in order to determine the relevant signaling molecules and the subsequent cellular pathways that are triggered. Various chemical, mechanical, and metabolic microenvironments have been shown to induce a wide range of angiogenic, anti-angiogenic, and maturation pathways. Eliciting the desired cellular responses requires precise control over the presence of specific biologically active cytokines and the cellular microenvironment as a whole. Recent innovations in micro-technology, advanced materials, drug delivery, and tissue engineering have enabled the precise manipulation of virtually all aspects of the cellular microenvironment. Microfluidics has shown exceptional promise due to the demonstrated ability to precisely control various parameters of the cellular microenvironment.

Therefore, microfluidic scaffolds enable one to indirectly incite a large set of desired cellular responses to direct or accelerate the *in vitro* growth of tissue or organs for regeneration applications.

1.5 Biomaterials

Polymeric, ceramic, and metallic biomaterials all play crucial roles in treatments and therapies of the medical industry. Specifically, biodegradable polymeric biomaterials have become instrumental in a wide range of novel technologies including drug delivery and tissue engineering. Recent advancements have focused on synthesizing unique polymer blends with properties that can afford advantages for specific bioengineering applications.

1.5.1 Role of Biomaterials in Tissue Engineering

Biodegradable polymers have significant potential in the fields of bioengineering. They have shown promise in drug delivery, *in vivo* sensing, and tissue engineering, the latter of which is of extreme interest in this study [34]. Biomaterials have been used in tissue engineering in the following ways:

1. The biomaterials are able to directly induce cellular migration and proliferation, which in turn results in tissue or organ regeneration.
2. Materials are used to encapsulate and segregate types of cell populations thereby functioning as a barrier between the implanted cells and the immune system.
3. Materials are fashioned into matrices used as a physical support for cell growth and organization into more complex hierarchal structures.

An example of the first approach involves the study of glycosoaminoglycan/collagen (GAC) constructs to stimulate healing and function as artificial skin. This approach has also been used in nerve and cartilage regeneration experiments[35]. The second approach fashions polymers into hollow

fiber membranes. Various types of cells can be placed within this membrane, which can then be implanted to treat a variety of organ failure problems[36]. This idea is also possible on a smaller scale. Macrocapsules fabricated from poly(acrylonitrile)-poly(vinylchloride) (PAN-PVC) membranes are able to encapsulate cells but contain pore sizes that are large enough to allow the transport of medium-sized molecules. The third application of biomaterials into tissue engineering utilizes a biodegradable scaffold to enable cellular proliferation and reorganization. Tissue engineering constructs made of biodegradable polymers are able to function as scaffolds for cell seeding and eventual implantation into a host[37]. One of the most widely studied polymers for this application is poly(D-lactic-co-glycolic acid) (PLGA), a biodegradable block co-polymer[38]. Substantial research has focused on fabricating a variety of scaffold geometries and compositions using PLGA. Sheets, fibers, and foams can all be produced and shaped into virtually any geometry. The large focus of work involving PLGA can be attributed in part to its FDA approval in addition to its various advantages. However, the fragile nature and poor mechanical properties of the polymer represent major limitations of PLGA as a biomaterial. Since most tissue engineering scaffolds will eventually be implanted into a biological system, the scaffolds will undergo many types of mechanical deformations and stresses. In addition to potential for mechanical failure of PLGA-based structures, exterior forces on an implanted rigid structure can cause local inflammation and scarring responses. As a result, ideal biodegradable tissue engineering scaffolds would be flexible with strong mechanical properties. Such a material would mimic the extracellular matrix (ECM), which is a tough, yet soft elastomeric network that provides stability and structural integrity to organs. Biomimicry of the soft ECM also reduces the effects of possible mechanical irritation to the surrounding tissues by allowing the implant to adjust to the dynamic stresses of the internal environment.

1.5.2 Existing Biodegradable Elastomers

Three classes of biodegradable elastomers have been previously reported: hydrogels[39], elastin-like peptides[40-42], and polyhydroxyalkanoates (PHAs)[43]. Hydrogels are water-swollen cross-linked networks composed of hydrophilic homopolymers or copolymers[44]. Hydrogels have proven to be extremely useful in the pharmaceutical and medical industries because of their high water content and elastic mechanical behavior. The primary advantage of hydrogels is their high degree of biocompatibility. This property is due primarily to the fact that the majority of the volume (~90%) of hydrogel formulations is water. Also, the specific properties of hydrogels can be modified by altering such characteristics as the chemical composition, dilution, and cross-linking density. However, one major disadvantage of hydrogels is the lack of mechanical strength as most hydrogel formulations exhibit an ultimate tensile strength on the order of 100kPa[45]. Also, hydrogels may exhibit a high degree of swelling which may prove to be useful in the synthesis of environmentally-responsive biomaterials. However, this characteristic limits the use of hydrogels as a material for fabricating biodegradable devices or structures that need to minimize swelling and maintain their geometry after implantation. Elastin-like peptides also show promise as a biodegradable elastomer. However, the method of fabrication is slow and expensive due to the need for genetic engineering of protein synthesis pathways. Producing large quantities of these proteins is also a time-consuming and costly endeavor. PHAs are inexpensive bio-polymer formulations that exhibit desirable mechanical properties[46]. However, there are significant drawbacks including the potential for large amounts of endotoxins found in industrial samples. Also, only some of the monomers of PHAs occur naturally within the body. The biocompatibity of PHAs is also suspect. Subcutaneous poly(3-hydroxybutyrate) implants lead to a variety of inflammatory reactions[47]. Macrophages, neutrophils, lymphocytes, and fibrocytes were all found immediately surrounding the implant. Thus far, the

established biodegradable elastomers all suffer significant drawbacks for use as biomaterials in treatments and therapies.

1.6 Poly(glycerol-sebacate)

1.6.1 Shortcomings of Existing Bio-Elastomers

Pre-existing classes of biodegradable elastomers have proven to be advantageous in a variety of applications including implantable porous scaffolds for tissue engineering. However, the fabrication of microfluidic tissue engineering scaffolds is unable to benefit from any of these materials. An implantable fluidic device must be biodegradable, biocompatible, tough, flexible, and fabricated with micron-scale precision. Hydrogels are not suitable because of their relatively low tensile strength. PHAs are only slightly biocompatible and elastin peptides are expensive and time consuming to synthesize. Furthermore, none of these materials have been molded into geometries with micron-scale features. Although PLGA has been molded into microfluidic devices[31], it is not flexible and could potentially cause scarring and inflammation upon implantation. Furthermore, PLGA has been shown to undergo bulk degradation *in vivo,* which results in microfractures and other defects that could impact the effectiveness of the device[48].

1.6.2 Poly(glycerol-sebacate) -- "Biorubber"

Poly(glycerol-sebacate) (PGS) is a recently developed material that offers many significant advantages for use in the development of tissue engineering scaffolds. PGS is a tough, biodegradable, elastomer that is biocompatible, inexpensive, and easy to synthesize. Inexpensive, ubiquitous starting materials and a bulk condensation polymerization process allow for large batches (~300 grams) to be synthesized. Sebacic acid and glycerol, the raw materials used in PGS synthesis, are found naturally in the body and have been FDA approved, respectively. In addition to these

advantages, PGS exhibits the desired mechanical properties of high elasticity and high strength (Figure 6). These characteristics are obtained through low-density covalent cross-linking and hydrogen-bonding interactions, which also give collagen and elastin their strength and elasticity. The ultimate tensile strength is approximtaley 0.5 MPa, significantly higher than hydrogels.

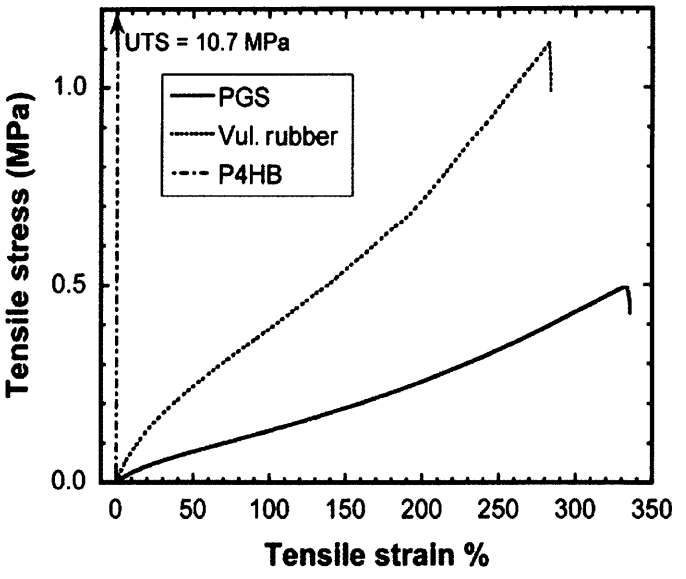

Figure 6. Stress Strain Curve of PGS compared to other materials[49].

PGS is biocompatible both *in vitro* and *in vivo*. In fact, cells seeded on PGS layers in culture exhibit increased proliferation and improved morphology when compared to other types of biopolymer layers. For example, 3T3 fibroblasts grown on PGS layers had more adherent cells and cells with normal morphology when compared to PLGA layers (Figure 7). Subcutaneous implants of PGS sheets into rats also show reduced inflammation and scarring when compared to PLGA implants.

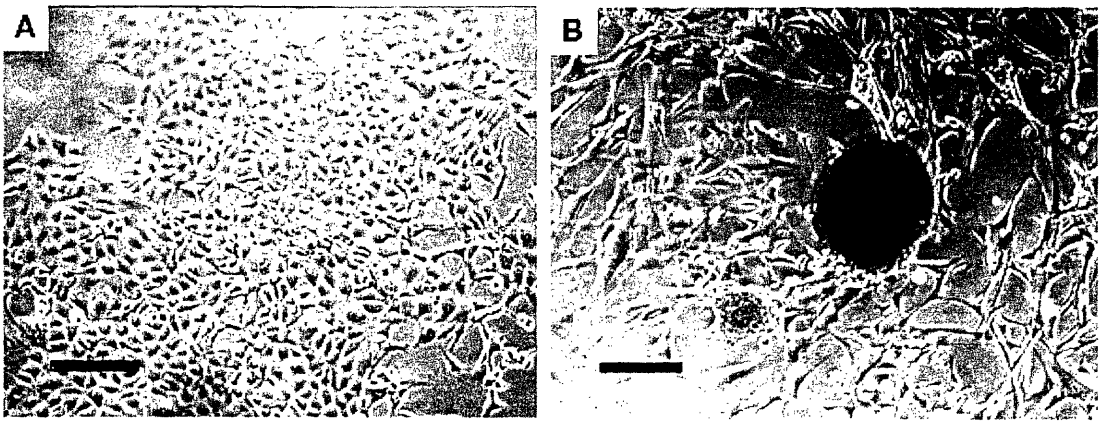

Figure 7. *In Vitro* Comparison of 3T3 Fibroblasts on PGS (A) and PLGA (B)[49]. Cells cultured on PGS layers exhibit increased proliferation and improved morphology when compared to cells cultured on PLGA layers.

The superior biocompatibility and mechanical properties suggest that PGS is a promising biomaterial for numerous medical applications. The biodegradability and elastomeric nature of PGS make this material an attractive platform for developing a variety of tissue engineering scaffolds.

Chapter 2: Measuring Transport Properties of Poly(glycerol-sebacate)

2.1 Introduction

Tissue engineering systems must be able to supply nutrients to cells seeded within the scaffold efficiently. As such, scaffolds fabricated out of various forms of PGS must be designed to overcome mass transfer limitations within the device. Therefore, one critical step in fabricating PGS-based microfluidic scaffolds is the assessment of the intrinsic mass transfer properties of the material. The transport characteristics of gases such as oxygen and carbon dioxide are especially important.

2.1.1 Rubbery vs. Glassy Polymers

There are two basic microstructural conditions of polymeric materials; the glassy and rubbery states. The mechanism of gas permeation through each of these types of polymers is very different. The main disparity between transport across rubbery and glassy polymers is due to the fact that glassy polymers are not in a true state of equilibrium. This non-equilibrium can result in significant differences in observed permeability and solubility coefficients. For example, diffusion coefficients in glassy polymers are highly non-linear functions of penetrant gas concentrations. Contrast this with the diffusion coefficients in rubbery polymers, which do not vary with changes in penetrant gas concentrations. Poly(glycerol-sebacate) our polymer of interest is a rubbery polymer at ambient temperatures of 22°C. Therefore, the focus of this transport study will concentrate on rubbery polymer systems. At temperatures above the glass transistion temperature (T_g), rubbery polymers are tough, flexible, which is associated with free chain motion[50]. Consequently, rubbery polymers have much shorter relaxation times, which allows them to immediately adjust to perturbations in

temperature or stresses. Rubbery polymers can therefore reach the new state of equilibrium very rapidly. This property is also applicable to the perturbation due to the absorption of a low molecular weight penetrant. In general, the penetrant diffusion is much faster in rubbery polymers relative to glassy polymers because of this rapid relaxation time. Altering the physical properties of the polymers, such as the crosslinking density, can modify the transport properties of both glassy and rubbery polymers. These alterations can, in part, lead to a wide range of experimental values when determining permeability coefficients. Therefore obtaining uniform PGS membrane samples will be of utmost importance when experimentally determining the relevant transport coefficients.

2.1.2 Theory

The mechanism of gas transport through a rubbery polymer membrane depends on many factors including the type of polymer. However, Graham's general solution-diffusion model suggests that there are three unique phases of gas transport through a membrane[51]; 1) Adsorption onto the polymer surface, 2) Diffusion through the bulk polymer, 3) Desorption into the external phase (Figure 8). These various microscopic mechanisms of gas transport can be manifested into three intrinsic macroscopic kinetic and thermodynamic properties; solubility, diffusivity, and permeability. The solubility coefficient is a thermodynamic property that relates the vapor pressure of the penetrant to the concentration of the penetrant in the polymer. The diffusivity coefficient is a kinetic property that describes the ability of a gas to penetrate the bulk polymer. The permeability is defined as the product of solubility and diffusivity and describes the intrinsic mass transfer resistance for a gas in a polymer membrane (k_m)[50]. However, there are also mass transfer resistances associated with concentration gradients in the gas feed ($k_{g,f}$) and gas permeate ($k_{g,p}$) which may need to be factored into calculating the overall mass transfer resistance across the membrane:

$$\frac{1}{K_{ov}} = \frac{1}{k_{g,f}} + \frac{1}{k_m} + \frac{1}{k_{g,p}} \qquad \text{(Eqn. 2.1)}$$

Assuming that the mass transfer resistance in the gas feed and permeate sides is negligible, the equation can be reduced to:

$$K_{ov} = k_m \qquad \text{(Eqn. 2.2)}$$

In other words, the permeability coefficient, P, relates the flux J and concentration gradient ΔC of the permeant species across a membrane of thickness δ, which is shown in the following expression.

$$J = P \cdot \frac{\Delta C}{\delta} \qquad \text{(Eqn. 2.3)}$$

For an ideal polymer system such as a rubbery polymer, these transport properties are constant with respect to pressure and concentration. PGS is classified as a rubbery polymer and, as a result, exhibits ideal transport behavior. Therefore, gas adsorption onto the polymer surface can be described by Henry's Law, which takes the following form:

$$C = S \cdot p \qquad \text{(Eqn. 2.4)}$$

where C is the concentration of the gas in the polymer, S is the solubility coefficient, and p is partial pressure of the penetrant in the gas phase. Diffusion of the gas in an ideal polymer occurs by the gas molecules creating channels and activating polymer chains within the bulk. These processes can be described macroscopically through the Poisson equation for mass transfer without reaction:

$$\frac{\partial c}{\partial t} = -D \cdot \nabla^2 \qquad \text{(Eqn. 2.5)}$$

This equation can be simplified for one dimensional diffusion to yield the following expression:

$$\frac{\partial c}{\partial t} = -D \cdot \frac{\partial^2 c}{\partial x^2} \qquad \text{(Eqn. 2.6)}$$

where D is the diffusivity and c is the concentration of the penetrant at time t and position x.

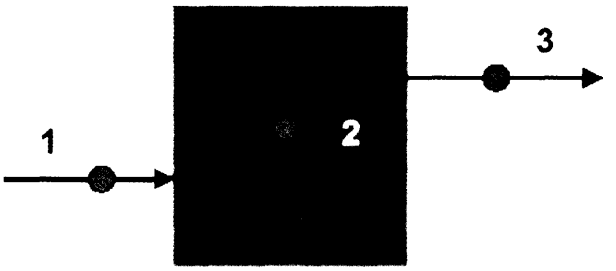

Figure 8. Three Stages of Gas Permeation. 1) Solution in polymer phase, 2) Diffusion across bulk polymer, 3) Desorption from polymer into external phase.

2.1.3 Measurement of Gas Permeabilities

One method of experimentally measuring the permeability coefficient P and the diffusion coefficient D of gases in polymer membranes is through a time-lag experiment[52]. These two properties can be used to calculate the solubility coefficient S, by the following relationship.

$$S = \frac{P}{D} \qquad \text{(Eqn. 2.7)}$$

This technique begins by positioning the membrane in a diffusion chamber such that there are separate upstream and downstream sides (Figure 9A). The membrane is initially evacuated of residual gases for several hours. At time $t = 0$, the permeant gas is supplied at the feed pressure P_{feed} and feed concentration c_i by opening valve a and continuous measurement of the downstream pressure P_d begins. A typical time evolution of downstream pressure P_d versus time t is shown in Figure 9B. Each experimental curve consists of both a transient state and a steady state. If an ideal membrane is free of penetrant at the start of the experiment, the amount of penetrant (Q_t) passing through the membrane in time t is given by[53]:

$$\frac{Q_t}{\delta c_i} = \frac{Dt}{\delta^2} - \frac{1}{6} - \frac{2}{\pi}\sum \frac{(-1)^n}{n^2} \exp\left[\frac{-Dn^2\pi^2 t}{\delta^2}\right] \qquad \text{(Eqn. 2.8)}$$

As $t \Rightarrow \infty$, the exponential term in eqn. 2.8 can be neglected as the equation simplifies to:

$$Q_t = \frac{Dc_i}{\delta}\left(t - \frac{\delta^2}{6D}\right) \qquad \text{(Eqn. 2.9)}$$

A simple linear extrapolation of the steady-state region, $\frac{Q_t}{\delta c_i}$ can be used to determine the time-lag θ, which can be used to calculate the diffusivity coefficient D via the following equation.

$$D = \frac{\delta^2}{6\theta} \qquad \text{(Eqn. 2.10)}$$

The steady state of the pressure versus time plot is used to calculate the permeability in a straightforward manner by manipulating the steady-state flux equation into the following form:

$$P = \frac{1}{P_{feed}} \cdot \frac{V_d M_{gas} \delta}{\rho \cdot RT \cdot A} \cdot \frac{dP_d}{dt} \qquad \text{(Eqn. 2.11)}$$

in which P_{feed} is the upstream penetrant pressure, V_d is the downstream volume, M_{gas} is the molecular weight of the penetrant gas at density ρ, and A is the membrane area. As previously mentioned, the solubility can be calculated once the permeability P and diffusion coefficients D are measured.

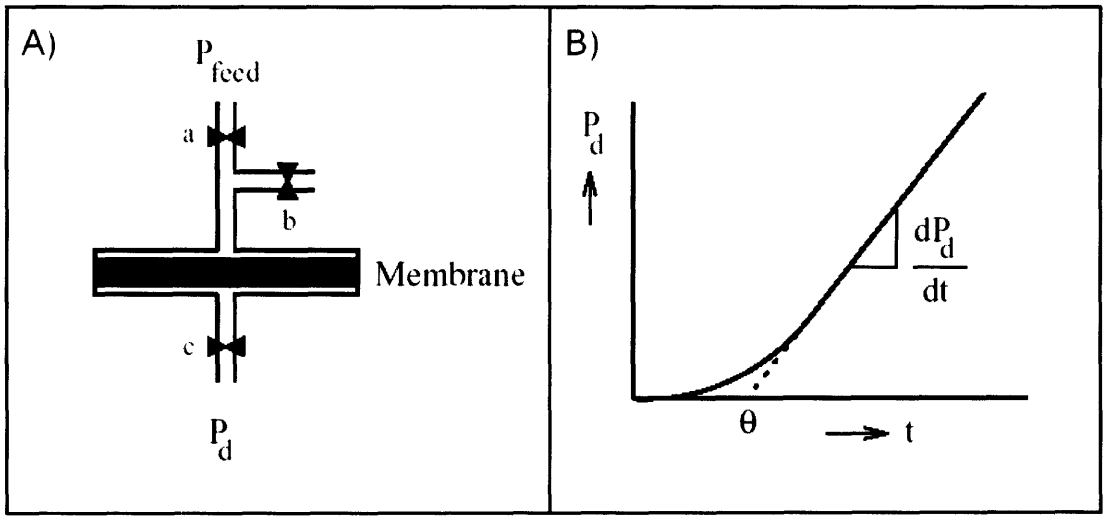

Figure 9. Time Lag Diffusion Experiment. A) Schematic of diffusion chamber with upstream and downstream valve networks. B) Time-evolution of downstream pressure (P_d). The steady-state slope of this profile is used to calculate the permeability of the membrane while the extrapolated time-lag θ is used to calculate the diffusivity. The solubility of the membrane can be calculated directly using Eqn 2.7

2.2 Experimental Methods

2.2.1 Time-lag Diffusion Experimental Apparatus

A schematic of the experimental set-up for measuring permeation by time-lag measurements is shown in Figure 10. The diffusion chamber is fabricated from two separate and identical pieces of 2024 aluminum (McMaster-Carr) that measure 3" x 3" x 1". Each piece contains a threaded inlet/outlet port, gas exchange chamber, porous supports for the membrane sample, and thru-holes for machine screw fasteners. The membrane sample is placed over the gas exchange area between the two aluminum pieces. A Viton R double-seal O-ring (McMaster-Carr) was placed around the outer diameter of the PGS membrane, which sealed off the sample from atmospheric gases. The upstream side of the diffusion chamber was connected to a poly(tetrafluoroethylene) (PTFE) tube

using Swage-Lok fittings. The pressure of the gas feed was regulated by a multi-stage regulator connected to a ¼" rubber hose complete with a Swage-Lok connection. The downstream side of the diffusion chamber was connected to a 1/8" NPT chrome-plated brass tube. The transducer used for pressure measurements was an MKS 902 Series Piezo Transducer with a K16 adapter by HPS Products. The pressure signal was recorded by a National Instruments 6035 DAQ card and inputted into LabVIEW 5.0. The vacuum source was supplied to the system by using a Welch 1402 DuoSeal Belt-Drive vacuum pump which was rated to 3 microns. The vacuum line consisted of ¼" rubber tubing connected to a stainless steel ball valves (McMaster-Carr) using a hose barb connection.

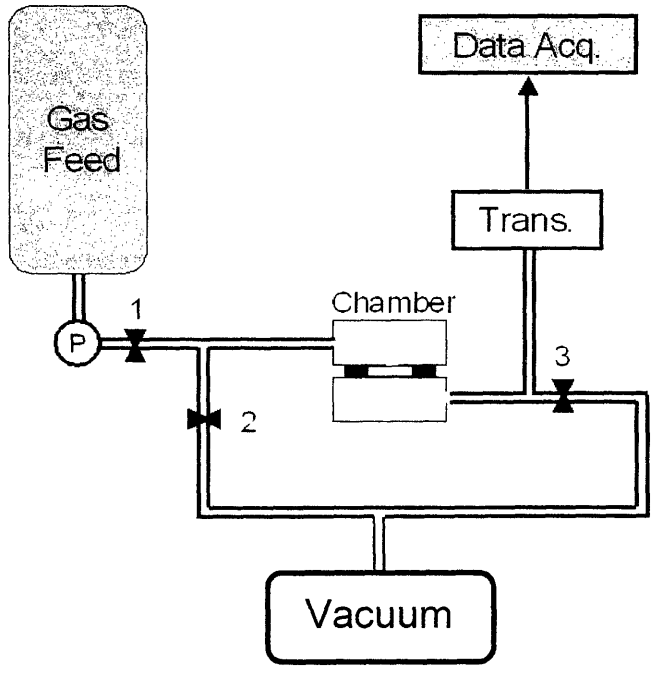

Figure 10. Schematic of Permeability Experimental Apparatus. PGS membranes were fastened within an aluminum diffusion chamber and sealed using a double-seal Viton O-ring. During membrane evacuation, valve 1 was closed and the vacuum was engaged. The pressure was manually monitored through the transducer to ensure that adequate vacuum was established. Data collection began by closing valves 2 and 3, opening valve 1, and establishing the appropriate gas feed pressure to the top side of the membrane. Data acquisition software was then used to take pressure transducer measurements every 3 hours.

2.2.2 Preparation of PGS Membranes

PGS is synthesized via the polycondensation of equimolar amounts of glycerol and sebacic acid (Figure 11). PGS features a hydrolysis degradation mechanism, an ester bond for chemical modification, a low density of crosslinking, and non-toxic monomers.

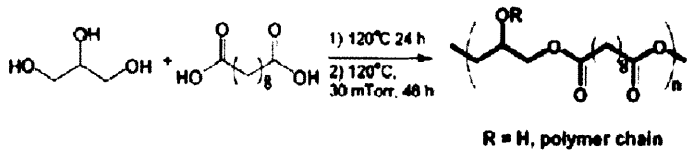

Figure 11. PGS Synthesis. PGS is synthesized via the poly-condensation of glycerol and sebacic acid. Heat and low-pressure aid in the removal of the water by-product during synthesis. The crosslinking density between polymer chains governs the high strength and elastic properties of PGS.

Sebacic acid (Sigma-Aldrich) used in PGS polymer synthesis was first purified by a crystallization procedure. 99% pure sebacic acid was dissolved in 200 proof dehydrated ethanol (Pharmco) at 70°C. The solution was cooled to -20°C for at least 12 hrs. The solution was filtered and the crystals were washed with chilled ethanol. The filtrate was discarded and the sebacic acid crystals were dried in an oven at 70°C. The PGS pre-polymer was synthesized by a polycondensation of an equimolar mixture of glycerol (Aldrich, Milwaukee, WI) and sebacid acid (Aldrich) at 120°C under nitrogen blanket for 24 hrs. The pressure was reduced from 760 torr to 300 mTorr over 5 hrs. The reaction mixture was then kept at 120°C and 40 mTorr for an additional 24 hrs. Glass substrates for PGS curing were prepared by rinsing with ethanol. A 90% (w/w) sucrose in water solution was placed on the substrate and spincoated at 1000RPM for 30 sec (Spincoater Model P6700, Speedline Technologies). The sucrose layer was baked at 120°C for 24 hrs. The PGS pre-polymer was then melted at 160°C and spread into thin films on a sucrose coated glass substrate. The polymer was cured at 150°C and 40 mTorr for 15 hrs. The substrate-polymer sample was then placed in DI water at 24°C for 24 hrs. Upon delamination, the PGS polymer membrane was removed from the mold, rinsed with ethanol and dried under vacuum for 24 hrs. The dried membranes were then stored in a desiccate environment at 24°C.

2.2.3 Time-lag Diffusion Experimental Procedure

PGS films thicknesses were determined by measuring at nine separate points across the entire sample with a micrometer (Mitutoyo). The PGS samples were cut to size (approximately 0.625" x 0.625") and mounted in the diffusion chamber. The first step in the diffusion experiment was the evacuation of the membrane of residual gases. This was achieved by closing valve 1 and opening valves 2 and 3. This allowed for the simultaneous evacuation of gases from both sides of the membrane. The pressure was monitored by manually recording measurements from the transducer throughout the evacuation process. The vacuum source was applied to both sides of the chamber and the membrane was evacuated for at least 120 hrs for all samples. After evacuation, the ball valve was closed and the vacuum source was stopped. The upstream chamber was immediately connected to the permeate gas feed line and purged for at least 5 min. The upstream pressure was then adjusted and sealed as data collection began. Data collection continued for at least 120 hrs. All of the permeation experiments took place at STP (24°C and 1 atm pressure).

2.3 Results

A set of permeation experiments was performed separately for both oxygen and carbon dioxide gases in PGS films. The diffusion coefficient D and permeability coefficient P were calculated from Eqns. 2.10 and 2.11 respectively. Using this information, the solubility S can easily be calculated from Eqn. 2.7. The results of these calculations are summarized in Table 2 and plotted in Figure 12. The values of the error bars are standard deviations of each set of sample measurements.

Table 2. Permeability, Diffusivity, and Solubility Coefficients of Oxygen and Carbon Dioxide in poly(glycerol-sebacate) at STP.

	Coefficient	Sample Size, N	Average, $\overline{X}$	Standard Deviation, σ	σ (%)
Oxygen	**P** x 10^{17} (m^3 STP-m)/(m^2-sec-N/m^2)	7	6.23	0.788	34.1
	D x 10^{12} (m^2/sec)	7	3.42	1.17	12.6
	S x 10^5 (m^3 STP)/(m^3-N/m^2)	7	2.03	0.792	39.0
Carbon Dioxide	**P** x 10^{17} (m^3 STP-m)/(m^2-sec-N/m^2)	3	13.6	3.44	22.8
	D x 10^{12} (m^2/sec)	3	2.15	0.490	25.3
	S x 10^5 (m^3 STP)/(m^3-N/m^2)	3	6.30	0.260	4.13

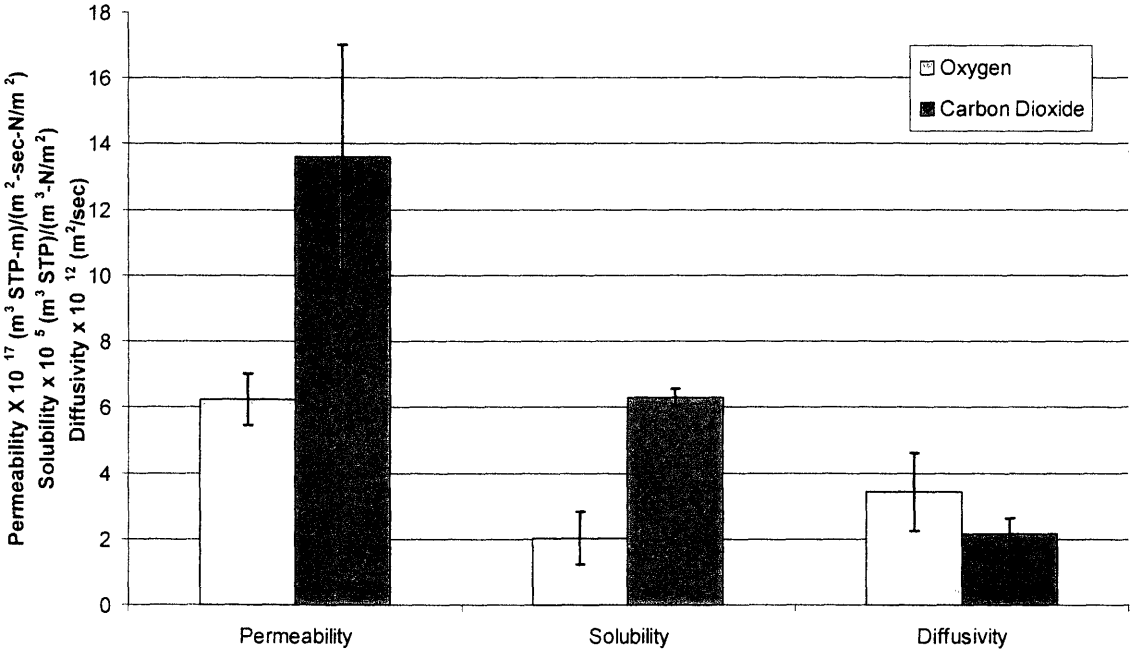

Figure 12. Permeability Solubility and Diffusivity of Select Gases Across PGS at STP under 1 atm of pressure differential. PGS membranes were more permeable to carbon dioxide than to oxygen. Carbon dioxide diffused slower, yet was more soluble in PGS when compared to oxygen.

2.4 Discussion

2.4.1 Explanation of Trends in Transport Coefficients

As is consistent with most polymer membranes, the diffusivity and solubility of the permeants in PGS membranes are directly related to the microscopic properties associated with each of the gases. The diffusivity of molecules in a polymer material is governed by the size of the permeant. Generally speaking, permeant gases with smaller solute sizes exhibit relatively high diffusivity coefficients. Conversely, smaller molecules exhibit relatively low diffusivity coefficients. This direct relationship between diffusivity and solute size is manifested in the following equation:

$$r = \frac{kT}{6\pi\eta D} \qquad \text{(Eqn 2.12)}$$

where k is the Boltzmann constant, T is temperature, and η is viscosity. Although this expression is only valid for large solutes, it can be used as a first-order approximation for smaller molecules such as gases. This equation can be used to determine the Lennard-Jones diameters of gases which are 0.337 nm and 0.40 nm for oxygen and carbon dioxide, respectively[53]. Now consider the solubility of gases in rubbery polymers. The solubility of a gas in a polymer is dependent upon the degree of interaction of the gas with the polymer. Furthermore, the interaction is a function of the solute, namely, the size of the gas. Therefore small gases such as helium, hydrogen, and even oxygen are considered to be non-interacting gases whereas carbon dioxide and other organic solutes can be classified as interacting. Higher diameter gases are able to condense more readily and are therefore more soluble in general[53]. PGS polymers are no exception as diffusion of gases in PGS is similar to ideal rubbery polymers. Carbon dioxide is found to have a much higher relative solubility and a slightly lower relative diffusivity in PGS when compared to oxygen. This can be attributed to the larger permeant diameter. Since the permeability, P, is governed by the expression $P = SD$, the resultant overall permeability of carbon dioxide is only moderately higher than oxygen.

2.4.2 Effect of Cross-linking on Measured Transport Coefficients

The high standard deviations in sample measurements can be attributed to the fact that the cross-linking density of PGS can vary significantly between membrane samples. As previously mentioned, the degree of cross-linking, in part, can have a large impact upon the measured transport coefficients. Therefore, there will be a large distribution of gas permeability depending upon the cross-linking density. The permeability of a given sample can be controlled to some extent by carefully monitoring the pre-polymer synthesis and curing steps. Even then, the conditions of these cross-linking steps can vary between samples. The cross-linking density is also dependent upon the stoichiometry of pre-polymer synthesis, which, in the case of PGS, calls for an equimolar mixture of sebacic acid and glycerol. Stoichiometic imbalances on the order of fractions of a percent can lead to significant variations in the cross-linking density[54]. In general, if the PGS membrane samples are cured at higher temperatures and lower pressures, a higher degree of polymerization occurs as more water is driven off during polycondensation and esterfication. This results in relatively high cross-linking densities, which in turn ultimately results in lower gas permeabilities. The age and storage conditions of PGS can also impact the transport properties in much the same manner as the selection of curing recipe. Typically, PGS prepolymer, as well as cured PGS samples, are stored in a desiccate environment to prevent the hydrolysis of the polyester bonds. However, the absence of water in the storage environment also drives esterfication. Hence, PGS samples that have been stored for a lengthy amount of time or PGS samples that are formed using older prepolymer formulations will contain a relatively high degree of cross-linking than newer samples and newer PGS formulations. Consequently, the transport properties can be significantly affected. This conclusion is both logical and intuitive. As the cross-linking density increases, the number of mean-free paths for a gas molecule decreases. This microscopic property has a direct impact upon the

macroscopic measurement, as the permeability will vary inversely with the relative degree of crosslinking.

2.4.3 Relative Permeability of PGS

One question that remains is how permeable PGS is relative to other common polymeric materials. In general, PGS was more permeable to gases than butyl rubber and less permeable than PDMS (Table 3 and Figure 13). The increased permeability in PGS relative to butyl rubber can be reconciled by the fact that both oxygen and carbon dioxide are more soluble and more mobile in PGS. However, an opposite trend is not responsible for the decreased permeability of both oxygen and carbon dioxide in PGS relative to PDMS. Rather, PGS exhibits a significantly higher solubility coefficient than PDMS because of the apparent increased activity of the penetrant with PGS. The overall permeability of the selected penetrant gases to PDMS is still much larger relative to PGS because of the increased diffusion coefficients. This large disparity in diffusivity can be attributed to the fact that PDMS is an unbranched, non-crosslinked, glassy polymer.

Table 3. Summary of Transport Coefficients of PGS Relative to Other Materials. Dimensionlesss coefficients for permeability, diffusivity, and solubility were calculated (i.e. $\underline{P} = P_{,PDMS}/P_{,PGS}$) to compare the properties of PGS to both butyl rubber and PDMS.

	Dimensionless Transport Coefficient	Butyl Rubber	PDMS
Oxygen	$\underline{P}$	0.18	72.86
	$\underline{D}$	0.26	876.68
	$\underline{S}$	0.62	0.25
Carbon Dioxide	$\underline{P}$	0.35	225.07
	$\underline{D}$	0.50	1136.36
	$\underline{S}$	0.71	0.20

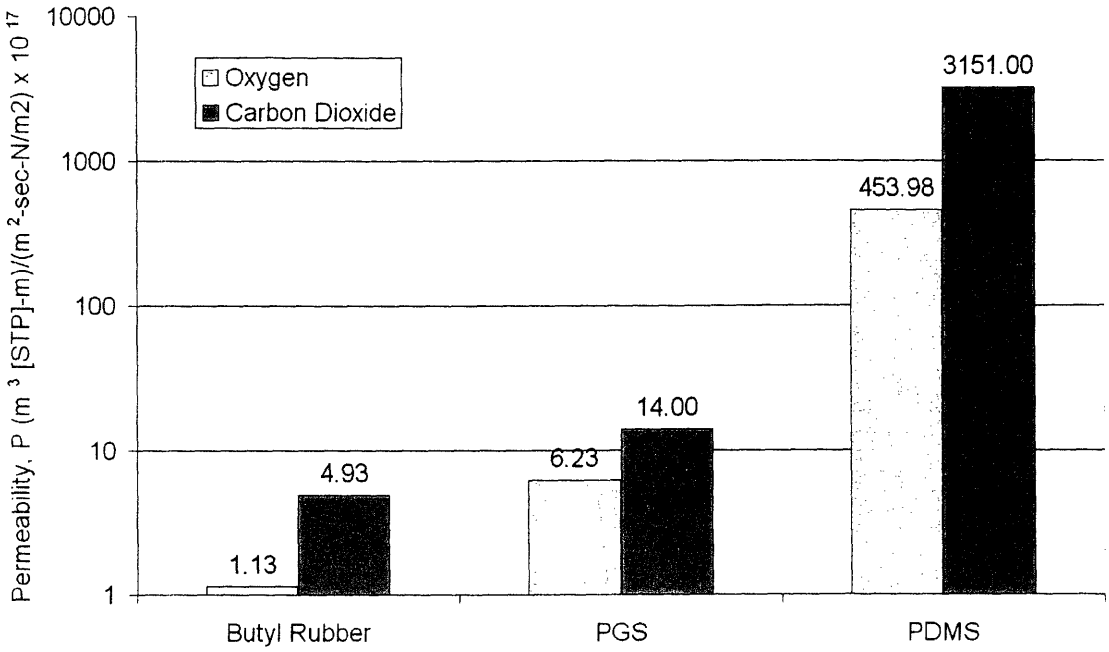

Figure 13. Relative Permeability of Oxygen and Carbon Dioxide in PGS. The permeability of PGS to both carbon dioxide and oxygen lie between that of butyl rubber and PDMS, a glassy polymer.

2.4.4 Design Applications and Summary

Determining the relevant transport coefficients of oxygen and carbon dioxide in PGS is a critical step in designing complex, multi-level tissue engineering systems. With this knowledge, it is important to determine a critical length scale for mass transport within PGS for designing solid supports with substantial volumes for tissue engineering applications. One potential mass transfer problem may involve the supply of oxygen across a layer of PGS to another layer of cells. A simple one-dimensional diffusion-reaction model can be used in the calculation (Figure 14). The objective of this calculation is to determine the maximum thickness of a PGS layer that ensures adequate oxygen supply to a cell monolayer through diffusion alone. Assuming an atmospheric feed concentration of oxygen, standard oxygen uptake rate (-4 nmol/min-10^6 cells) and cell density for a confluent cell layer, as well as a defined hypoxic limit of 5 μM, the appropriate thickness can be

calculated by flux matching of diffusion and oxygen consumption shown respectively in the following calculations:

$$J_{diff} = \frac{Perm \cdot \Delta P}{\delta} = [6.23E\text{-}17\ (m^3\ STP\text{-}m)/(m^2\text{-}sec\text{-}N/m^2)*(0.2*101325\ -373)N/m^2]/\delta\ mol/m^2\text{-}sec$$

$$J_{O_2,cons} = (\text{Cell Density})(\text{Consumption Rate}) = (5.66E9\ cells/m^2)*(6.67E\text{-}11\ mol/sec\text{-}10^6\ cells)$$

It is also necessary to assume rapid equilibrium of oxygen with the PGS membrane and rapid consumption at the surface of the cell monolayer. The results of this calculation suggest that a PGS membrane thickness δ of approximately 27 microns is necessary to satisfy the aforementioned conditions. Even though the actual value could vary across the PGS membrane or the cell type used, the minimum thickness should not vary beyond an order of magnitude of the calculated length scale. Even if the most ideal conditions for transport were achieved, the fabrication of high-volume, solid PGS tissue engineering scaffolds would lead to hypoxic regions throughout the device if appropriate precautions are not taken. First and foremost, it is difficult to fabricate and manipulate thin layers of PGS with consistent accuracy. Furthermore, this calculation assumes oxygen consumption for only a single cell monolayer. Presumably, many layers of cells will be seeded in a future PGS-based tissue-engineering device. Also, it will be necessary to support cells with more than merely the hypoxic limit if rapid growth and proliferation are desired.

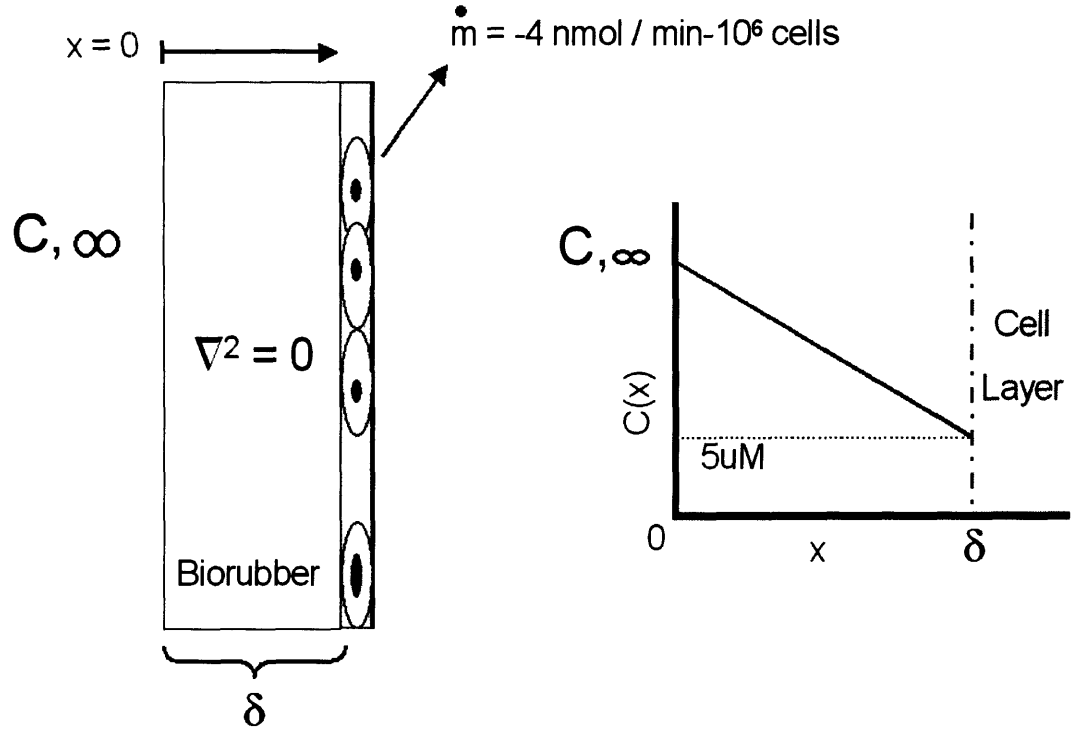

Figure 14. Diffusion-Reaction Model For Oxygen Supply to Cell Monolayers Across PGS Membranes. This simple model was devised to calculate the maximum allowable thickness of PGS sheets to supply a monolayer of cells with a concentration at or above the hypoxic limit. This model makes several assumptions including the rapid equilibrium of oxygen gas between air and water along with general parameters of cells including physical dimensions and oxygen uptake rates. The maximum thickness of PGS membrane was found to be 27 microns.

Therefore, it is possible to conclude that complex, multi-layered PGS-based tissue engineering devices will require additional measures to support seeded cells. One possible solution could be the addition of an in-line oxygenator to infuse the media with high concentrations of oxygen. The sheets of PGS could also be modified to contain pores or channels using a variety of methods to aid in convective oxygen supply to the cells. Doing so will also allow the efficient supply of other nutrients such as glucose as well as larger signaling molecules such as VEGF and EGF, which play crucial roles in the proliferation and maturation of blood vessels. Despite the mass transport

limitations of solid PGS scaffolds for mutli-layered tissue engineering scaffolds, solid PGS is a suitable material for fabricating simple scaffolds in which mass transport limitations are not present.

Chapter 3: Fabrication and Endothelialization of Simple PGS Microfluidic Scaffolds

3.1 Introduction

3.1.1 PGS-based Tissue Engineering Scaffolds

One formidable challenge of tissue engineering complex organs is the adequate supply of nutrients and removal of metabolites. One of the limiting factors in engineering complex organs such as the liver and kidney is the lack of an intrinsic blood supply. Hepatocyte cell culture is a very challenging task in itself. Furthermore, simply seeding a porous scaffold with hepatocytes and parenchymal cells will not result in a functional liver. Therefore, in an effort to create a biomimetic microenvironment, it is desirable to establish a co-culture of hepatocytes and parenchymal cells in combination with an established microvasculature. There has been a wide range of polymer processing techniques designed to form templates of appropriate length scales for cell seeding and tissue growth[55]. The spatial resolution of such techniques as 3-dimensional printing (3DP) is on the order of 200 microns[56]. Although this resolution is sufficient for many types of tissue engineering applications such as skin, and cartilage, it is not appropriate for vascular tissue engineering applications. The majority of the cross-sectional area of the circulatory system exists in the capillary beds. These vasculature structures have diameters on the order of 10 microns[30], rendering 3DP insufficient for fabricating scaffolds to support capillaries, a critical component of the circulatory system. This limitation can be overcome by the recent application of MEMS fabrication techniques to tissue engineering, such as standard silicon micromachining, replica molding, and microfluidics. The primary objective of this research is to fabricate microfluidic scaffolds and biodegradable BioMEMS devices for blood vessel tissue engineering applications using PGS. PGS is a thermoset polymer, which can be molded with micron-scale precision. The pre-polymer is soluble in a number

of common organic solvents allowing PGS to be shaped into virtually any desired geometry. These characteristics make PGS a promising material platform for fabrication of biodegradable BioMEMS devices for use as an implantable microvascular tissue engineering scaffold. The approach for fabrication of PGS-based microfluidic devices mimics the fabrication of PDMS microfluidic devices. Although creating prototypic microfluidic devices using PDMS is rapid and relatively simple, using PGS to create biodegradable scaffolds has proven to be more difficult. However, both processes utilize standard microfabrication techniques to produce a negative mold with micron-scale feature resolution. A PGS polymer with a low cross-linking density is cast over the mold and cured to induce further crosslinking. The molded, highly-crosslinked PGS polymer is delaminated from the mold. This patterned polymer layer is then bonded to an un-patterned, partially cross-linked PGS layer thereby forming the complete microfluidic device. A schematic of this process is shown in Figure 15.

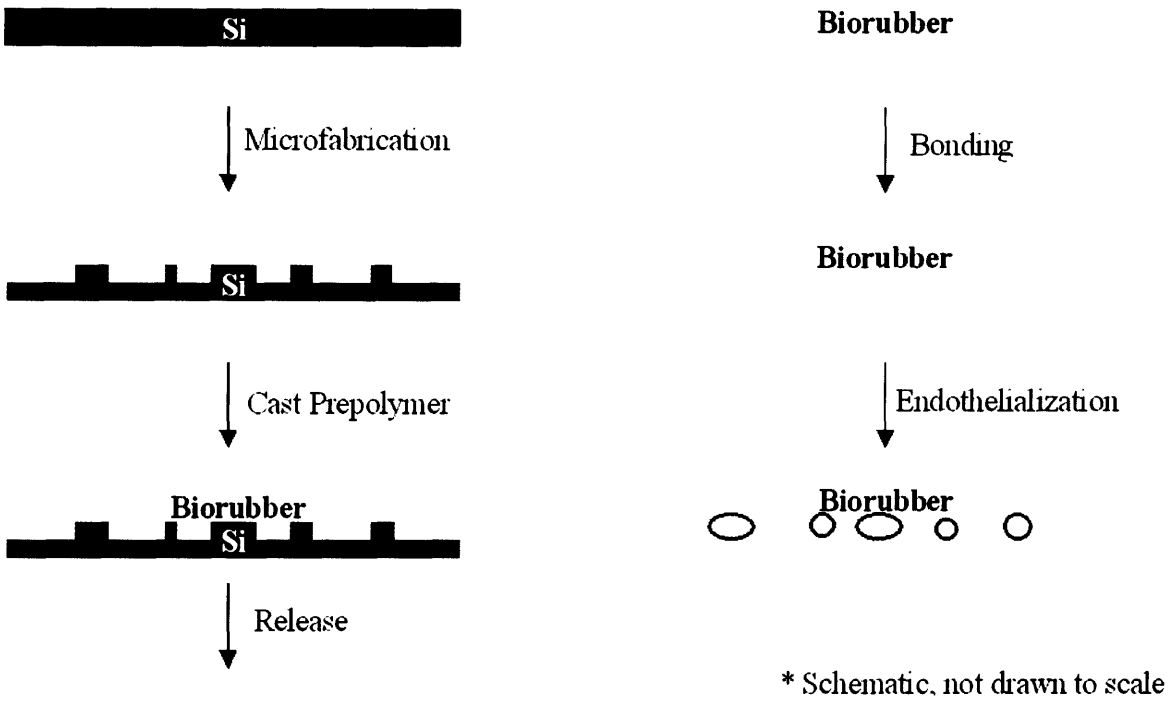

Figure 15. Process Flow for Fabricating PGS Microfluidic Scaffolds. After silicon micromachining and adding a sacrificial sucrose release layer, the PGS pre-polymer is cast on the mold. The PGS is cured, released, and cleaned. The patterned layer is then bonded to a semi-cured unpatterned PGS layer and the entire device undergoes another curing step to bond the two layers. Fluid connections are made (not shown) and subsequent cell culture takes place.

3.2 Materials and Methods

3.2.1 Microfabrication of Bulk Silicon Microfluidic Masters

Established microfabrication technologies have been able to produce features with dimensions that are on the order of 0.1 microns. This precise feature resolution is more than sufficient for producing features in scaffolds to support capillaries. The first step in producing microfluidic tissue engineering scaffolds is the fabrication of a master, which is a negative mold for polymer casting. The photolithography implemented in this work was designed to produce a "negative mold". In other words, the appropriate pattern contains raised channel features on an etched background. The microfluidic pattern was designed as a solution to a computational fluid dynamics problem with

several design rules (Figure 16). One design rule imposed on the system was that 85% of the cross-sectional area of flow had to be contained within the capillaries. In general, the microfluidic network aimed to maximize the capillary density while also achieving flow characteristics and geometries that approximated those of native capillary beds.

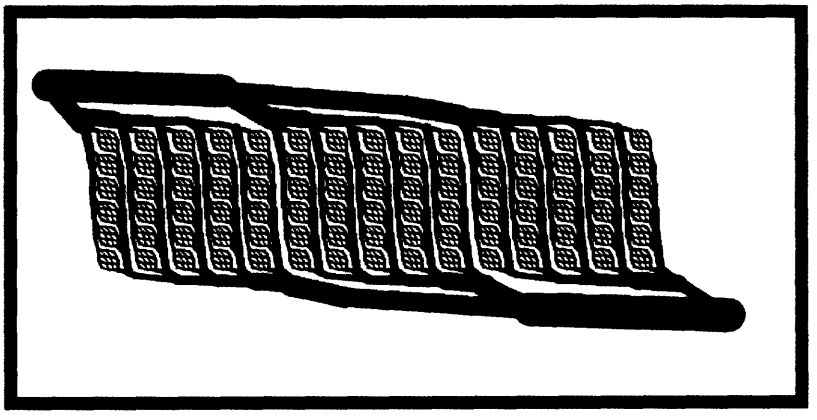

Figure 16. Photolithography Mask for Microfluidic Master. This mask layout was used to fabricate bulk-etched silicon microfluidic masters for PGS casting and curing. The design was intended to achieve a uniform shear stress and flow rate throughout the capillary beds. 100 mm wafers were able to contain two die of this size.

Plasma etching of silicon is a widely used process in the fabrication of both integrated circuits as well as MEMS. More specifically, high aspect ratio micromachining (HARMS) is a powerful tool that features superior control over the spatial resolution and feature size. These advantages make HARMS a well-suited process for fabricating microfluidic masters. One issue in using microfabricated devices for biological applications is the possibility of sharp angles within the devices. Cell culture experiments have suggested that these salient features lead to poor lining and coverage of endothelial cells. However, this issue is resolved through the application of a thin (less than 3 microns) sacrificial sucrose release layer of which details will be discussed in the following section.

3.2.2 Fabrication of PGS-based Microfluidic Scaffolds

Replica molding using poly(di-methyl siloxane) (PDMS) on silicon masters is an established process for creating microfluidic devices for biomedical applications. However, the aggressive nature of PGS pre-polymer prevents simple replica molding directly on silicon masters in an identical manner as PDMS. Prior to PGS casting, silicon masters were piranha and plasma cleaned. A sacrificial sucrose release layer was then applied to the surface of the cleaned silicon masters. A 90% (w/w) sucrose water solution was filtered through a 0.22 micron filter (Millipore) and was spun at 1000 RPM for 30 seconds and quickly dried by placing the wafer on a hot plate at 65°C for 60 seconds. The sucrose layers were then baked at 120°C for 24 hrs.

PGS pre-polymer was synthesized from purified sebacic acid and glycerol and applied to the sucrose-coated silicon master. The polymer was melted at 160°C ($T_{m,PGS}$ = 120°C) and evenly spread over the wafer. The PGS was cross-linked at 150°C and 40 mTorr for 15 hrs. The PGS was delaminated from the master by sucrose dissolution, rinsed with ethanol, and dried under vacuum for 24 hrs. The unpatterned layer of the microfluidic device was fabricated in a similar manner. Briefly, glass slides were cleaned with rinsed with ethanol and dried. PGS pre-polymer was melted at 160°C and spread evenly across the slide to from a thin layer of approximately 1 mm thick. The polymer was then semi-cured at 120°C for 28 hrs. Inlet and outlet sections were cut and removed from the unpatterned layer to allow fluid connections to the device. The patterned layer was then pressed down against the semi-cured layer gently to form a seal. The microfluidic device was fully assembled and sealed using an additional curing process. 23 gauge and 20 gauge luer stub adapters (Intramedic, Becton-Dicksenson) were used as the inlet and outlet connections respectively. The inlet and outlet regions surrounding the needles were sealed with polyurethane (McMaster-Carr). Luer-lock connections (0.063") were made to silicone tubing (ID: 0.063", OD: 0.125", Masterflex).

3.2.3 Endothelialization and Cell Culture

PGS microfluidic scaffolds were sterilized as a result of the conditions of the final bonding process of the two PGS layers. A G-RDG-S peptide solution (50 μg/mL in 1X PBS (Gibco)) was perfused through the device to aid in the cell attachment and proliferation. The device was incubated for 1 hr at 37°C and 5% CO_2 to equilibrate the device and allow for G-RGD-S adsorption. Human umbilical endothelial cells (HUVECs) (Cambrex) in their 3rd or 4th passage were harvested to concentrations of 1 x 10^7 cells/mL with EBM media and EGM-2 growth factor kits (Cambrex) using prescribed cell culture techniques. Cell suspensions were condensed to 1 mL and manually injected into the device using a syringe. The seeded cells were incubated under static conditions for 4 hrs to allow for cell attachment. After 4 hrs, the device was set up in a linear bioreactor system, which consisted of a syringe pump and 20 mL media reservoir, microfluidic scaffold, and waste container. The rate of perfusion was kept steady at 200 μL/hr and the reservoir was recharged with media as necessary. Continuous non-pulsatile perfusion of media was maintained for the majority of the duration of the experiment. The flow was only stopped to obtain images and recharge the media supply.

3.3 Results

3.3.1 Characterization of PGS Microfluidic Devices

An example of a fabricated PGS microfluidic device is shown in Figure 17. The transparent nature of PGS allows for easy observation during subsequent procedures such as preparation, seeding, and perfusion culture. The inlet and outlet ports are located at the upper left and lower right respectively. Polyurethane was used to seal the inlet and outlet ports. The dimensions of the microfluidic device and supporting glass substrate are 75 mm x 38 mm x 2.75 mm (L x W x H).

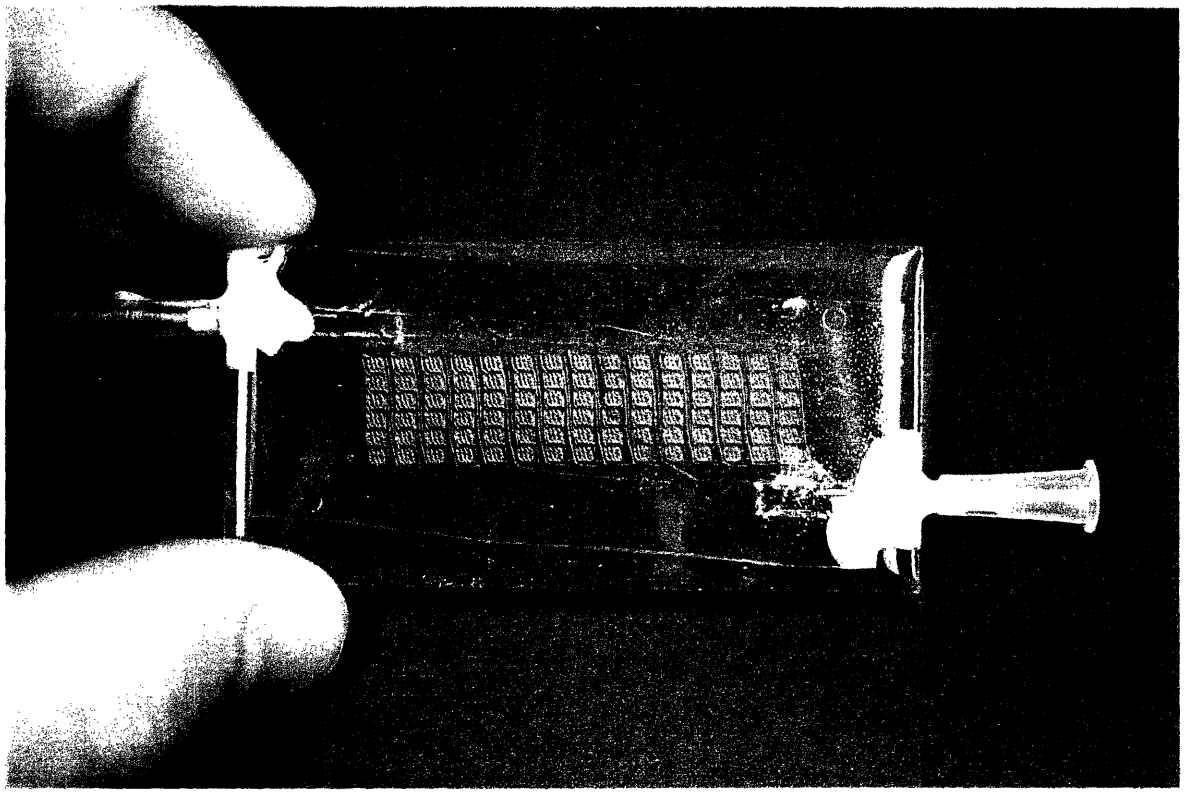

Figure 17. A Completed PGS-based Microfluidic Scaffold. The inlet and outlet ports are located at the upper-left and lower-right respectively. Polyurethane is used to seal the inlet and outlet ports. The dimensions of the scaffold and supporting glass substrate are 75 mm x 38 mm x 2.75 mm (L x W x H).

The two-dimensional network of capillaries was designed with several considerations. Critical aspects of physiological networks were featured such as the distance between capillaries as dictated by diffusion limitations, scaling laws for branching and dimensional changes, and overall pressure drop over the network. Additionally, wall shear stress, pressure drop, etc. were kept as uniform as possible using predictive fluid mechanic simulations. The results of those simulations are shown in Figure 18.

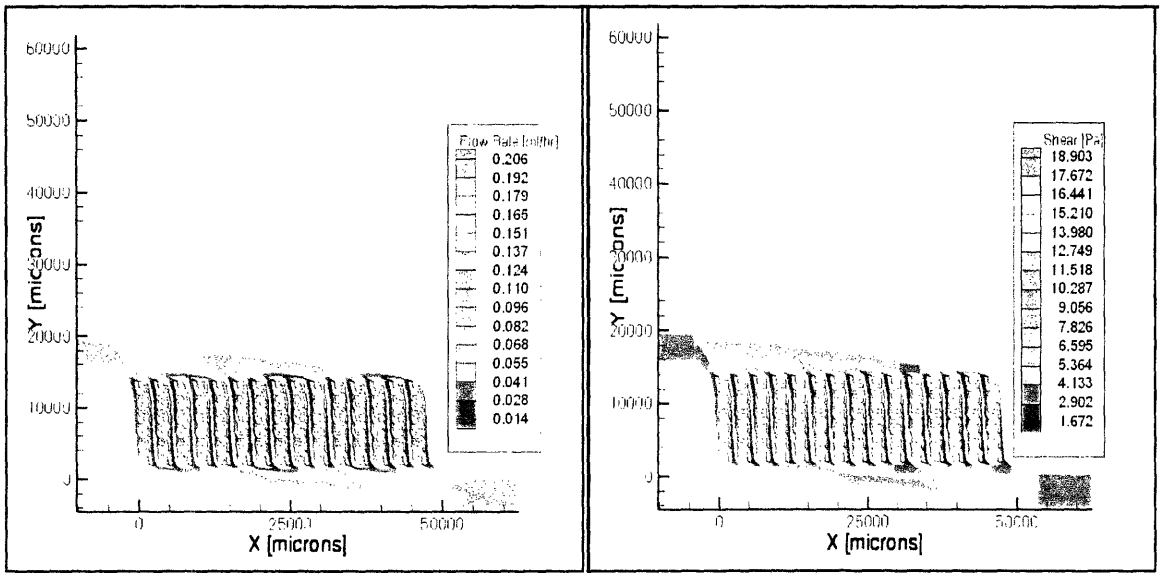

Figure 18. CFD results of microfluidic network at an inlet volumetric flow rate of 200 μL/hr. The flow rates and shear stresses were variable in the larger channels at the inlet and outlet, but were constant in the capillary bed regions of the microfluidic device.

The microchannels of the device are bonded without leakage or occlusion (Figure 19A).

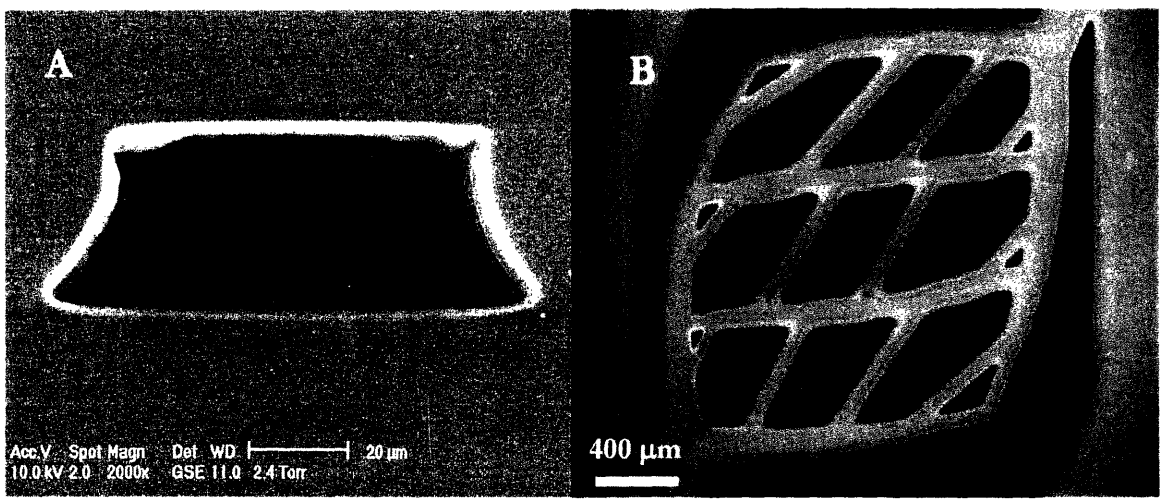

Figure 19. Characterization of PGS Microchannels. A) SEM cross-section of PGS microfluidic channel. B) Top-down view of rhodamine flowing through sealed microchannels demonstrating the absence of leakage or occlusion.

3.3.2 Vascuarlized PGS Microfluidic Scaffolds

Upon seeding, viable HUVECs appeared to attach to portions of the microfluidic device within 2 hours of static seeding (Figure 20A). Initial cell attachment was primarily isolated to channels with low flow rates and to the stagnation points of bifurcations. As perfusion was started, the cells began to proliferate from their initial islands of attachment. After 7 days of perfusion cell culture, regions of confluent cells were observed in capillary channels. Cell coverage remained somewhat sparse for the larger channels. Cells were grown in culture for up to 14 days (Figure 20B, C, D).

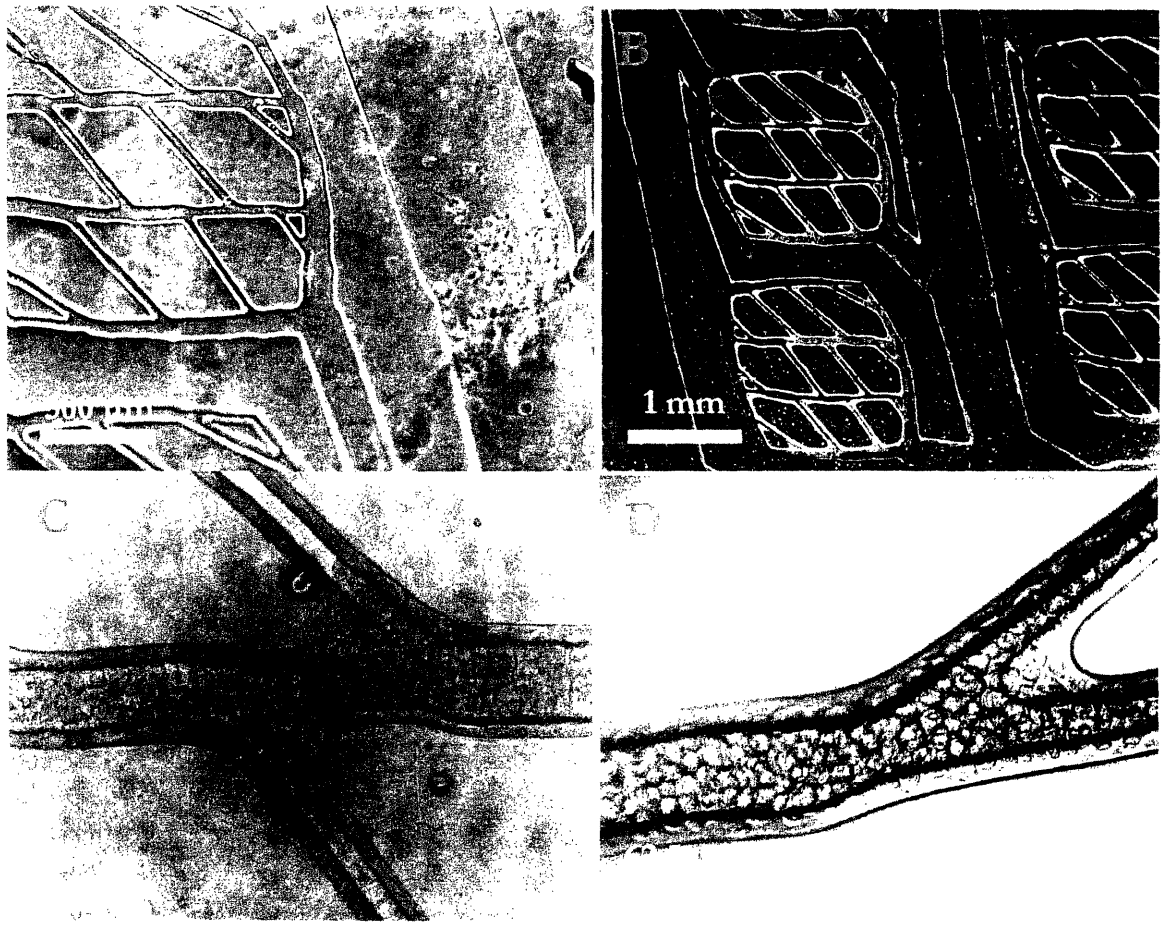

Figure 20. Endothelialization of HUVECs in PGS Microfluidic Scaffolds. A) Initial static seeding of HUVECS, 5X. B) Partial confluence after 14 weeks of perfusion cell culture at 2.5X. C) 20X. D) and 40X.

3.4 Discussion

Perhaps one of the most critical issues in fabricating microfluidic devices is the strength of the bonding between the layers, as this is often a problem for PDMS-based systems. However, the ability for PGS to cross-link has resulted in high strength bonding between PGS layers. These chemical bonds are strong enough that failure of the material often occurs before delamination. This results in hermetically sealed microchannels that can handle high-pressure liquids effectively. The junction between the patterned and unpatterned layers is virtually indistinguishable in the SEM cross-section of a typical microchannel (Figure 19A). In fact, the highest incidence of device leaks occurred at the sealed connections at the inlet and outlet ports during high pressure fluid flow. Improved fluidic connections to the device will be a requirement for fabricating devices more efficiently with higher yields. This packaging problem parallels similar problems of the microelectronics industry. Namely, much of the effort in the fabrication of the device is focused on designing and developing the internal architecture of the device. However, many difficulties can occur when attempting to interface the micron-sized device with the macroscopic systems that support the device. Future improvements may be able to microfabricate devices with connections that are suitable for both cell culture and an eventual artery shunt procedure. The ideal materials used in these connections should be biodegradable as well.

Microchannel Geometry. The height of the microchannel shown in Figure 19A was measured to be approximately 26 microns. Note that this is significantly shorter than the original feature height of 35 microns that was etched into the microfluidic master. There are two possible causes for this disparity. One minor factor may be the non-uniform thickness of sucrose layers on the raised features versus the etched substrate. It may be possible that the sucrose solution accumulates on the

substrate resulting in a thicker layer and a reduced effective feature height of the PGS replica mold. However, the most significant cause can be attributed to the depression of the fully cured PGS patterned layer into the semi-cured PGS unpatterned layer. There is very little control in this process as there are many factors that can affect the channel height including the degree of polymerization of the semi-cured layer and the force applied when sealing the two layers together. Overcoming this issue and effectively controlling the height of the microchannels is a critical issue because of the effect of the cross-sectional area on the fluid mechanics. Variations in height could lead to deviations between predicted and experimental fluid mechanic environments, which in turn could affect the proliferation and maturation of endothelial cells. The microchannels also have a trapezoidal cross-sectional geometry instead of the expected rectangular shape. The presence of "feet" can be attributed to a sucrose-wetting artifact during the spin coating of the sacrificial sucrose layer. The junction of the raised features and substrate causes the sucrose layer to accumulate along the corners. The increased local amount of sucrose results in a thicker layer and therefore impacts the final geometry of the PGS replica mold. These feet are also visible in the top-down photographs of the PGS microchannels during cell seeding and perfusion (See Figure 20D). There are two prominent lines that are located parallel to the cell-seeded microchannels. The inner line is the channel width at the top of the microchannel and represents the ideal channel dimensions. The outer line is the width of the channels at the base of the microchannel and represents the increased dimension of the channels as a result of the previously described sucrose-wetting artifact. Although this characteristic can result in non-physiological channel geometries and inaccuracies between theoretical fluid mechanical simulations and actual experimental conditions, these deviations from ideal replica molding have proven to be beneficial in some regards. The area in proximity to microchannel bifurcations exhibits the largest differential between channel dimensions. In addition to the stagnation of fluid flow in these regions, the large, somewhat occluded microchannel serves to

promote the initial adhesion of cells during seeding by increasing the amount of surface area. Additionally, the bifurcations also function as regions of circulatory flow. As previously described, oscillatory shear stresses associated with circulatory flow are found to increase the expression of vascular cell adhesion molecule (VCAM-1). Therefore, the increased vascularization near bifurcations can be attributed to local increased concentrations of VCAM-1.

HUVEC Perfusion Culture. Seeded HUVECs were able to attach to the microchannels of the PGS scaffold due, in part, to the RGD peptide preparation. After several days in culture, the cell population expanded to confluence in the capillary beds as well as near-confluence in larger channels. This initial success of perfused HUVEC cell culture within microfluidic PGS scaffolds is encouraging. The incorporation of cells with microfluidic devices has been the subject of intense study for a wide range of applications. However, this work has established the successful long-term culture in a biodegradable and biocompatible microfluidic system. This long-term culture protocol will be required to obtain devices with 100% confluence because of the spatial limitations that the microchannels impose on cell proliferation. At any point in time, only the cells that are located at the leading edge of the cell monolayer are proliferating and expanding. Consider the typical culture of animal cells in T-flasks. Assuming a moderate to high seeding density, a confluent monolayer of cells can be obtained within a few days as the number of cells on the leading edge that can proliferate increases. This leads to rapid radial expansion to form a confluent layer very rapidly (Figure 21A-C). Contrast this situation to cell expansion in a microchannel. Instead of a ring of proliferating cells on the leading edge, only a limited number of cells are able to proliferate. Therefore, in the case of cell culture within a microchannel, many more cell divisions must take place in order to obtain a confluent layer as the cells can only expand linearly along one axis (Figure 21D-F).

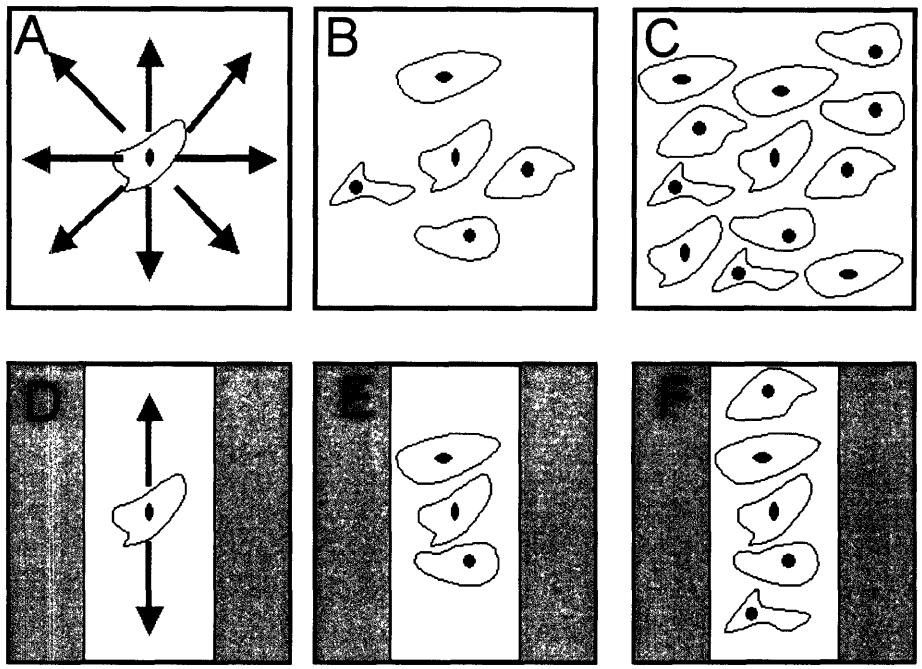

Figure 21. Spatial Constriction of Expansion of Cells in Microchannels. A-C) Cells proliferating in culture dish are able to expand in all directions producing a confluent layer of cells very rapidly. D-F) Increased time for proliferating cells in microchannels to achieve a confluent layer.

3.4.1 Flow Rates and Fluid Mechanics in PGS Microfluidic Scaffolds

One critical parameter that must be optimized is the perfusion rate. At low flow rates, cells may not be receiving enough nutrients. However, high flow rates will result in increased wall shear stress, which in turn may damage or remove cell monolayers from the walls of the microchannel. These free-floating cells may form clumps and subsequently occlude channels. Further complication in identifying the optimum flow rate arises from the need to obtain physiological flow characteristics. Even though the length scales and flow geometry of the microfluidic network may mimic natural capillaries accurately, the ultimate behavior of the fluid within the channels is also dependent upon the chosen flow rate. Therefore, it may be impossible to find a global optimum flow rate for cell growth given the coupling of the issues of cell adhesion, nutrient supply, and physiological flow

conditions. The chosen flow rate of 200 μL/hr produces a shear stress of approximately 20 dynes/cm^2 in the capillary bed region of the microfluidic device. This shear stress corresponds to moderate arterial flow in physiological systems[15]. Ideally, the shear stress could be reduced (~2 dynes/cm^2) by lowering the volumetric flow rate, but hypoxia and nutrient depravation may occur at such minimal flow rates. A mathematical model that can simulate fluid mechanic behavior of the media within the microfluidic device as well as the rate of cellular oxygen and nutrient consumption would be required to calculate the optimal rate of perfusion in this complex system. It may even be possible to precisely control the flow rate such that a near-hypoxic oxygen concentration can be achieved during the initiation of cell culture. This could lead to the rapid increase in local angiogenic factors via the HIF-1 promoter. Other possible improvements to the perfusion system might be the incorporation of a fluidic circuit and a pulsatile flow system. A perfusion circuit would circulate media from a large media reservoir to the microfluidic bioreactor and recycle the media back to the reservoir. The system could be supplemented with an in-line oxygenator and bubble trap to condition the media before entry into the reactor. A peristaltic pump installed in a circuit would be able to effectively circulate the media. Additionally, this type of pump would provide a sinusoidal pressure waveform. As previously mentioned, these dynamic shear stresses could lead to upregulation of angiogenic factors within cells.

Yet another complication of creating a biomimetic environment is the difference in the fluid mechanic properties of media and blood. Media can be approximated as a Newtonian fluid, which can greatly simplify computational fluid dynamics (CFD) of *in vitro* systems. However, blood exhibits non-Newtonian rheology. Hence, the actual *in vivo* hemodynamics is much more complicated and, as a result, can deviate from microfluidic cell culture systems designed using CFD. These subtle differences can impart extremely different signals to cells via mechano-transduction

triggering a wide range of cell fates from apoptosis or quiescence to proliferation and angiogenesis. Therefore, controlling the mechanical microenvironment within the microchannels is critical along with other aspects of the tissue-engineering scaffold.

3.4.2 Summary and Future Direction

The long-term culture of HUVECs was demonstrated in microfluidic devices that were fabricated from PGS, a novel biodegradable elastomer. Partially confluent layers began to form within the microchannels during the continuous perfusion. Fully confluent layers could be achieved if sufficient time for cell-culture was allowed. Angiogenic factors could easily be incorporated into the system in addition to soluble growth factors within the media. Perhaps the most exciting aspect of this project is the potential for scalability and integration of this fundamental system to make organ regeneration a reality in the foreseeable future. In the previously described work, simple single-layer microfluidic devices were fabricated from PGS and seeded only with HUVEC cells. However, similar methods can be employed to fabricate multi-layered devices that are connected together to form a tissue engineering scaffold with volumes on the order of cm^3 (Figure 22). Dozens of microfluidic chambers could be stacked vertically to allow sufficient transport of nutrients via perfusion since the device is so thin (2.75 mm). The surface area coverage of the each device layer can be increased just as easily by simply scaling up the layout of the 2-D microfluidic master.

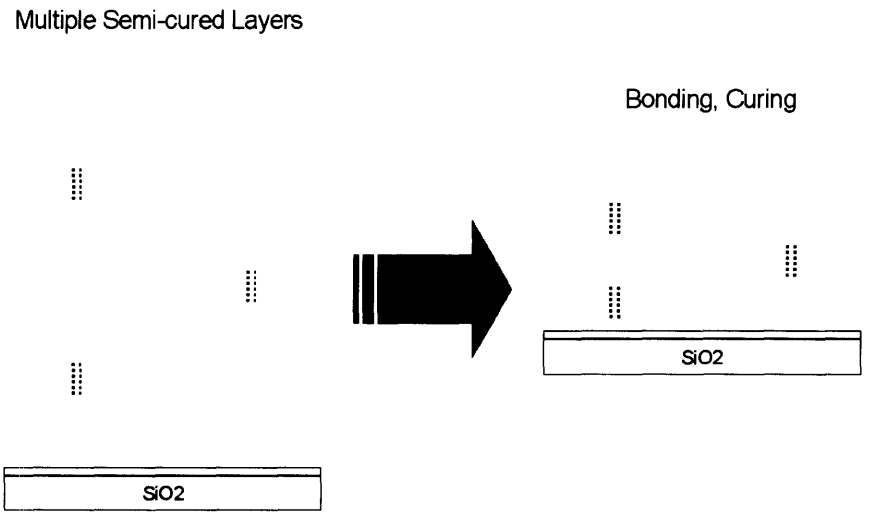

Figure 22. Cross-sectional Schematic of Fabrication of a Multi-Layered PGS Microfluidic Scaffold. Multiple replica-molded semi-cured PGS layers are modified with vertical connections to layers located immediately above and below. These multiple layers can be aligned and joined using an additional curing step to form a multi-leveled microfluidic network.

Furthermore, additional cell types can be co-cultured in addition to HUVEC or other endothelial cell lines. For example, hepatocytes and parenchymal cells can be introduced into the tissue engineering scaffold and grown in the presence of the pre-existing vascular network. PGS can also be modified using a number of standardized techniques. PGS foams with pore sizes on the order of 150-200 microns can be synthesized using a salt-leaching method. In general, this work will function as a springboard for large, more advanced PGS-based scaffolds that will aid in the regeneration of complex organs and tissues with intrinsic vascular networks.

Chapter 4: Fabrication of Complex PGS Microfluidic Scaffolds

4.1 Introduction

4.1.1 Channel Height Constraints in Bulk-Etched Silicon Masters

Microfluidic devices are commonly fabricated using replica molding of silicon substrates for a variety of applications. One characteristic of these systems is that the channel or feature height is uniform across the entire device. Depending upon the specific application or material, the lack of flexibility in microfabrication is oftentimes inconsequential. However, fabricating microfluidic devices for microvascular tissue engineering applications by replica molding via a master with a uniform feature height is undesirable for numerous reasons. The root cause of these problems is the extremely large aspect ratios that are present in channels located near the inlet and outlet regions. These channels must have large cross-sectional areas in order to meet the fluid mechanic specifications of uniform flow rate and shear stress. Ideally, the cross-sectional geometry of these large channels would be a square and the area of the smaller channels could simply be scaled up or down as necessary. However, the height of the capillaries and the inlet/outlet channels must remain constant because of the silicon etch process. Therefore, the inlet/outlet channel height become small to accommodate the capillaries, which compose the majority of the device. One direct problem with this fabrication technique is the potential for sagging and occlusion of the large channels due to the flexible nature of PGS. This problem can often ruin the entire device and reduce yield substantially when fabricating multiple devices. Another direct consequence of this problem is the presence of non-physiological channel geometries. Vascular systems found in nature feature a series of circular arteries with diameters that are scaled down in predictable increments. Rectangular channels with

non-uniform aspect ratios are not biomimetic of a microvascular system. The fabrication of a microfluidic device that more accurately mimics natural vasculature would be beneficial for tissue engineering applications.

4.1.2 Microfabrication Using Novel Three-Dimensional Electroplating Technique

Multi-leveled MEMS devices can be fabricated using a simple electroplating technique[57]. The process, which is similar to LIGA, is used to selectively electrodeposit metals to conductive islands that are patterned on an insulating substrate. . The conductive patterns, which are usually composed of Au (111) layers that are on the order of 5000A thick, are deposited on silicon nitride or silicon oxide substrates using a standard lift-off process. A wire is bonded to the first conductive island and the entire substrate is placed in a standard electroplating solution. Initially, nickel is only deposited on the portion of the wafer that is in electrical contact with the bonding wire. As plating progresses, the nickel pattern extends isometrically until electrical contact is made with the following conductive pattern. At this point, nickel is plating on both conductive islands isometrically. The plating continues to form a sequence of geometries that have subsequently smaller feature heights and smaller cross-sectional areas, but uniform aspect ratios. A schematic of this process is shown in Figure 23. The potential for creating scaled features with uniform aspect ratios is an attractive feature that makes this technique a suitable method for producing microfluidic scaffolds for vascular tissue engineering applications (Figure 24).

The most critical design components of these systems are the width of the conductive islands and the distance between them. In combination with the amount of electrodeposited nickel, these

parameters govern the final channel geometry by defining the relative aspect ratio and height of the features of the master. Since electrodeposited nickel adds approximately uniformly and isometrically, calculating the theoretical geometries is elementary. Consider the following general system:

The height of the n^{th} feature is given by:

$$H_n = \sum_{n}^{N} d_{i-1} + d_i f \qquad \text{(Eqn 4.1)}$$

where N is the gap number currently plating and f is the fraction of gap N that has already been plated. Similarly, the width of the n^{th} feature is:

$$W_n = W_o + 2\sum_{n}^{N} d_{i-1} + d_i f \qquad \text{(Eqn 4.2)}$$

where W_o is the width of the conductive pattern line segment. From these equations, it is clear that aspect ratios (defined as W/L) of ~2 occur as W_o approaches 0 and as the summation of all the gap distances becomes large. Therefore, it is advantageous to fabricate conductive patterns with the smallest line width possible. Theoretically, current photolithographic technology can produce line widths on the order of 1 micron. In addition to expensive mask processing, there are a number of other difficulties associated with patterning at such a high resolution. Consistently fabricating pattern line widths on the order of 25 microns is more cost effective and more time efficient in terms of processing while simultaneously achieving a high yield. Equal in importance to the gap distances is the actual topography of the conductive islands on the insulating substrate. Producing biomimetic flow geometries is critical in developing an effective microvascular tissue engineering scaffold. However, utilizing the electroplating technique of the microfluidic master restricts the design possibilities. Consider the electrodeposition of nickel on a long, narrow conductive island. The region proximal to the voltage source will be subjected to a higher current relative to distal

regions as a result of voltage drop across the segment. This results in non-uniform plating. Moreover, these non-uniformities will become exacerbated as plating continues because of the dynamic resistance of the segment. As the feature increases in surface area, the resistance will decrease, which in turn will increase the local current density. Therefore, regions that experience a higher current density initially will add nickel more rapidly thereby decreasing the local resistance to further increase the current density in that region. This positive feedback nature of electrodeposition both demonstrates the importance of fabricating features that are initially uniform and impacts the nature of the design layout. For simplicity, it is advantageous to minimize the spatial variation of branching locations along a given conductive pattern for the previously mentioned reasons. This qualification can be manifested in a design rule that requires layouts to possess bisecting horizontal and vertical lines of symmetry.

Perhaps the most important parameter in electrodeposition is the current and voltage that is applied across the conductive islands and the counter-electrode. In general, electroplating processes dynamically adjust the voltage in order to apply a constant current (galvanostat mode). Typical electroplating processes supply current densities on the order of 1 mA/cm^2 which is able to deposited nickel at the rate of 100 nm/min. These processes are generally used to deposit thin layers of nickel or copper. However, the previously outlined process requires large amounts of nickel deposition in order to build up large feature sizes. Since the area for nickel deposition increases significantly as a function of time over the electrodeposition, the current density of the system is changing even if a constant current is applied. Therefore maintaining a constant, uniform current density requires integration with a control system. Although maintaining the current density over the course of the process would be ideal, it is not critical in this specific application of fabricating microfluidic masters. It is more important to minimize roughness on the nickel surfaces.

As previously mentioned, the current density will gradually decrease over time as the amount of electrodeposited nickel increases and as a gap junctions between conductive islands are connected. Therefore, the effect of decreasing current density can actually serve to be beneficial. Namely, the highest current densities associated with the initiation of electrodeposition will result in a relatively high surface roughness. However, the increased surface roughness of the nickel is inconsequential as it is more important to build up the volume of the raised features at this point in the process. As the electrodeposition process concludes, the current densities will be significantly smaller, which results in a smooth surface.

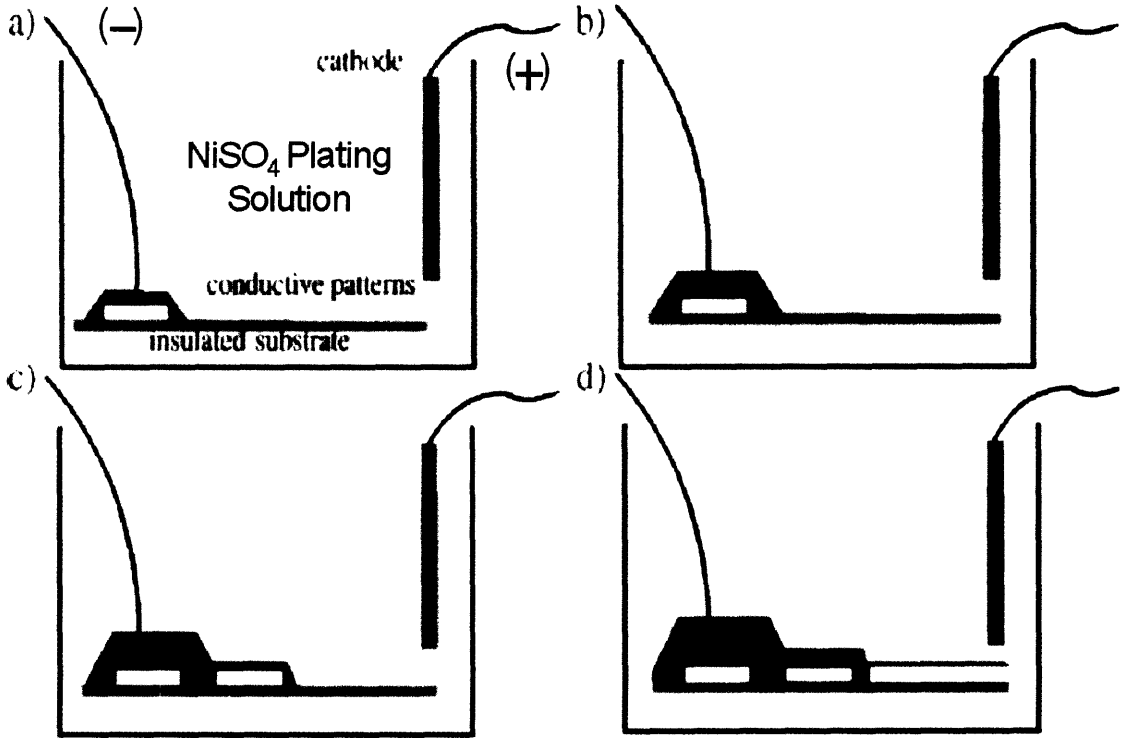

Figure 23. Three-Dimensional Electrodeposition of Nickel[57]. Microfluidic masters with variable feature heights can be fabricated using this LIGA-based method. The substrate to be electroplated consists of a pattern of conductive islands on an insulated layer. When plating initiates, only the pattern that is in electrical contact with the wire-bond begins to plate (A). As the Nickel extends isometrically, another island will be brought into electrical contact (B), allowing for both islands to begin plating (C). This step repeats for subsequent islands (D) resulting in an array of patterns with variable feature height.

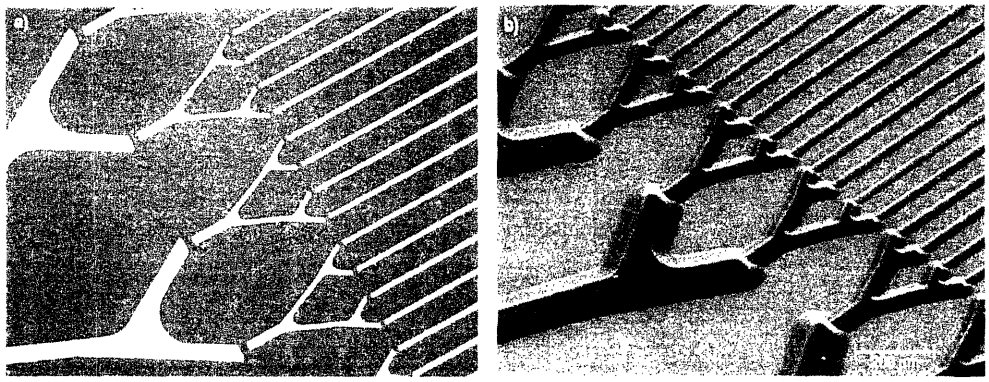

Figure 24. Fabrication of Microfluidic Master for Vascular Tissue Engineering Applications[57]. A). Au (111) conductive patterns on silicon nitride substrate prior to electrodeposition. B) SEM of electroplated microfluidic master fabricated using polypyrrole. A nearly identical process can be used in the fabrication of nickel masters.

4.1.3 Ultra-thin Layers of PGS

One of the most critical factors in designing a tissue engineering system is the efficient mass transport of nutrients and waste products. In Section 2.4.4, the length-scale of oxygen diffusion limitations was calculated to be 27 microns. Therefore fabricating PGS layers with this thickness will be required to maintain sufficient oxygen supply to cells seeded in solid PGS scaffolds. There are additional advantages of fabricating thin layers of PGS with thicknesses on the order of 20 μm such as minimizing aggregate thickness of multi-layered PGS systems. Therefore, fabricating PGS microfluidic scaffolds with wall thicknesses on the order of 20 microns is instrumental in the success of complex tissue engineering systems for the *in vitro* regeneration of vascularized organs such as the liver or kidney. Heating PGS pre-polymer above T_m and manually spreading the liquid can produce layers on the order of 1 mm. PGS layers < 1 mm in thickness can be produced by applying two established methods. Spin coating techniques, which are often used in the fabrication of MEMS devices, can also be used to achieve thicknesses of various liquid polymers on the order of microns. Also, drawing liquid polymer solutions using a doctor blade can attain thin layers of similar

thicknesses. Both techniques will be explored in the following section. These thin PGS layers can then be used to complete the microfluidic device.

4.2 Materials and Methods

4.2.1 Microfabrication of Gold Patterned Substrates

A standard Gold lift-off technique was used to pattern conductive islands on a thermal oxide substrate[58]. The layouts (Figure 25) were generated with AutoCAD software. DXF files were printed on to transparency masks (International Phototool Company), which were then converted to chrome-on-glass masks. The microfabrication of the plating template begins with chemical vapor deposition (CVD) of 3000A of silicon oxide. Photoresist was patterned on the wafer (Shipley 1827 photoresist, Shipley 351 developer) followed by the deposition of a 400A thick layer of titanium (DC Magnetron Sputter), which was initially applied as an adhesion layer. A 5000A layer of gold was then deposited to enhance the conductivity of the patterns. The metal layers that were deposited on the photoresist were removed during the lift-off etch (Shipley 1112A). The wafers were then rinsed with ethanol and acetone.

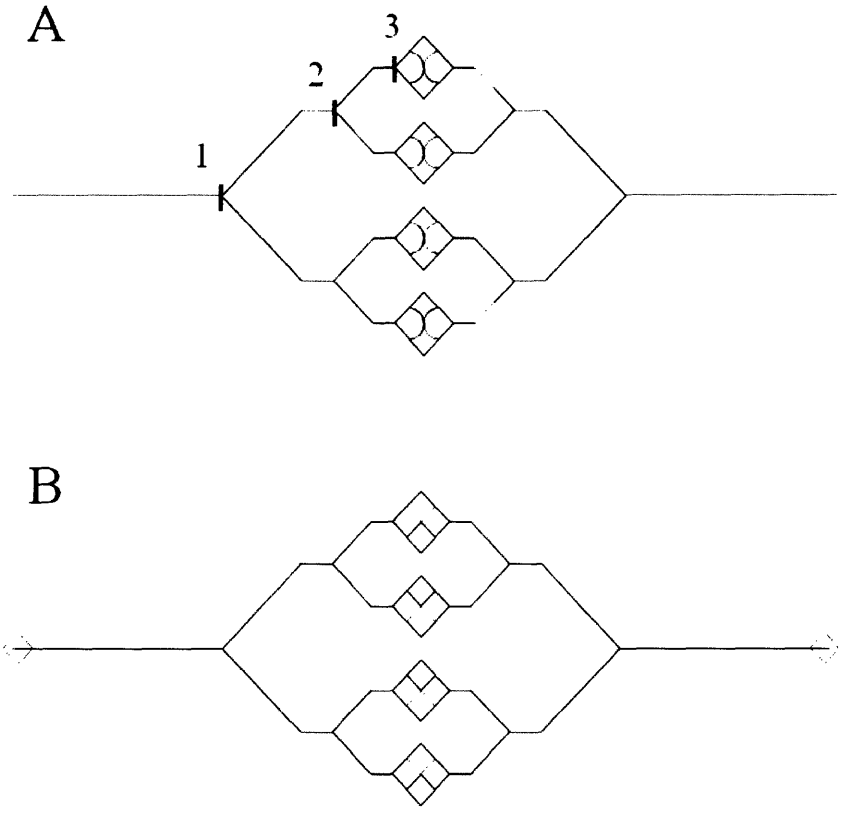

Figure 25. Individual Layouts for Microfabrication of Electrodeposited Substrates. The layouts were designed to have four levels segments with gaps of specific lengths at the representative locations shown above. The gap locations are symmetrical about the x-axis and y-axis and are in identical locations for both patterns.

Table 4. Summary of Gap Distances Between Conductive Islands in Layouts in Microns.

Gap #	Layout A	Layout B
1	20	25
2	20	20
3	15	20

4.2.2 Electrodeposition of Nickel

Two wire leads were bonded to wafers on two initial conductive islands using a silver colloid solution (Electron Microscopy Sciences), which was cured for 24 hrs at 24°C. The wire-bonded area was then coated with an insulated acrylic polymer (M-Coat D), which was cured for 1 hr at 75°C.

The wafers were cleaned again with tape and rinsed with ethanol and water to remove additional particles. The plating solution selected for electrodeposition was the Watt's bath, a nickel sulfate and nickel chloride-containing solution that also contains surfactants to assist in smooth plating. The counter electrode was a commercially pure Alloy 200 Nickel bar (McMaster Carr) with dimensions 12" x 2" x 1/8". Plating was performed using standard procedures using the Watt's bath formulation at 50°C[59, 60]. Substrates were plated at initial voltages of 0.5 V in a potentiostat setting with initial current densities ranging from 0.5 mA to 0.7 mA. The total duration of plating ranged from 48 hrs to 72 hrs depending upon the die pattern, gap distances, and desired overall feature height. Substrates with layout A were plated for 48 hrs while substrates with layout B were plated for 72 hrs.

4.2.3 Feature Metrology

Upon completion of the electrodeposition process, the measurement of features height was completed using a micrometer (Mitutoyo). For those samples that were not selected for future PGS molding, the electrodeposited nickel was removed from the substrate to enable measurement of the widths of the microchannels as well. The width of the features was measured using a Zeiss microscope (software by Axiovision) at 2.5X magnification.

4.2.4 Micromolding of Poly(glycerol-sebacate)

The casting and curing of PGS on electrodesposited microfluidic masters is identical to molding using silicon micromachined masters (See Section 3.2.2). Briefly, the die are rinsed with ethanol and plasma cleaned. The die are then spin-coated with a sucrose-water solution (90% w/w) at 1000RPM for 30 sec. The sucrose is pre-baked on a hot plate at 65°C for 1 min and then fully cured at 120°C for 24 hrs. PGS pre-polymer was then melted on the die at 160°C and cured at 150°C and 40 mTorr for 15 hrs. The PGS was delaminated from the wafers via sucrose dissolution in DI H_2O for 24 hrs

at 24°C. PGS layers were rinsed with ethanol, dried under vacuum for 24 hrs, and stored in a desiccator.

4.2.5 Synthesis of Ultra-thin Layers of PGS

Two methods of producing ultra thin films of PGS were employed. Spin coating PGS polymer was completed by first melting the pre-polymer using a heat gun (Pamran Co.) at temperatures above 120°C. The appropriate amount of melted pre-polymer was poured on to a sucrose-coated substrate to aid in the release of the PGS layer. The substrate was then mounted on the spin coater. Recipes were varied to achieve different film thicknesses. Speeds ranged from 250-750 RPM with a processing time of 30s. Applying heat constantly during spincoating is necessary to maintain constant viscosities. The second method used a 4" doctor blade (Gardco) to draw out thin layers of pre-polymer on sucrose-coated substrates. Appropriate amounts of PGS pre-polymer were melted and poured on to substrates. The doctor blade height was adjusted according to the desired film thickness and drawn across the substrate while the pre-polymer was still melted. Thin layers of PGS were cured in a vacuum oven at 150°C and 40 mTorr for 15 hrs (See Section 2.2.2). Layers were delaminated in DI H_20, rinsed with 200 proof ethanol and dried in vacuum. Thickness measurements were made using a micrometer (Mitutoyo) at eight different locations across the membrane. Thin PGS layers were also used to fabricate thin-walled PGS-based microfluidic devices to overcome oxygen transport limitations. The schematic for thin-walled device fabrication is shown in Figure 26.

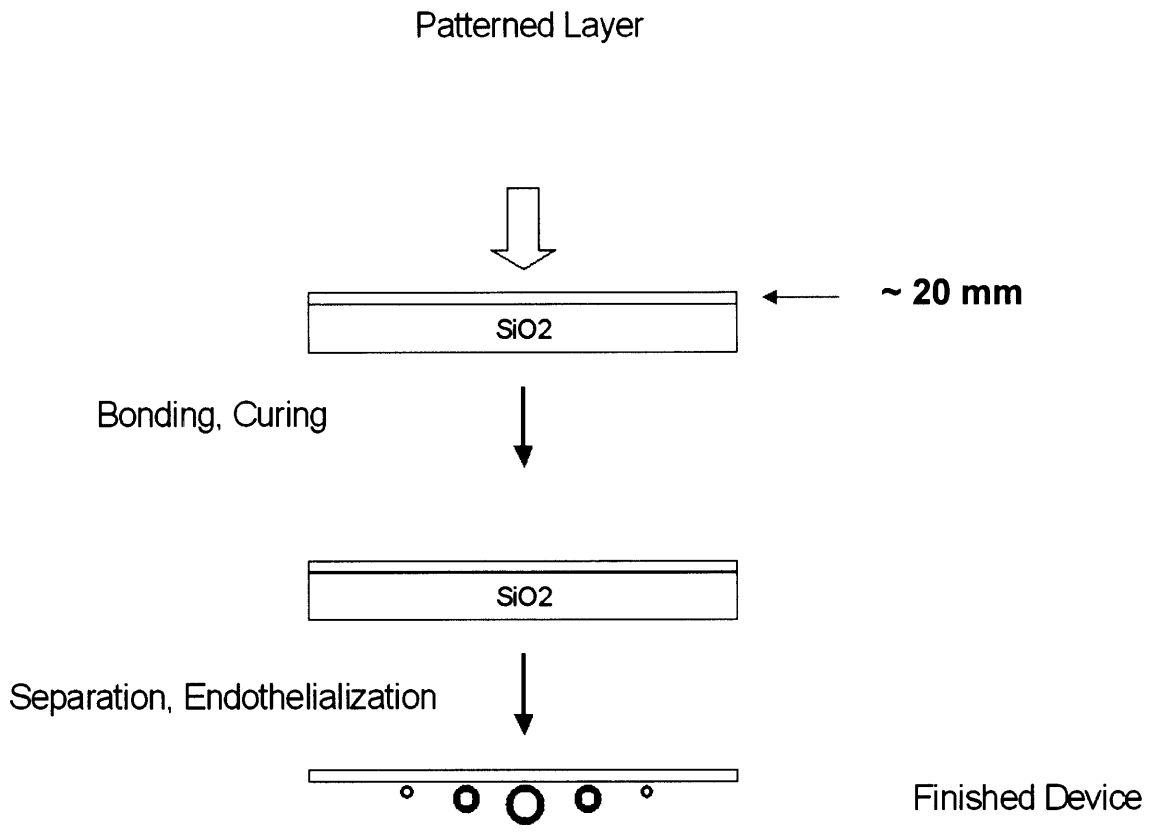

Figure 26. Fabrication of Thin-Walled PGS Microfluidic Tissue Engineering Scaffolds.

4.3 Results

4.3.1 Multi-level Electrodeposited Nickel Microfluidic Masters

Nickel deposited molds that contained were successfully produced using the previously described protocol. Figure 27 illustrates the progression of nickel electroplating for Layout A. The channel dimensions of the electrodeposited mold for Layouts A and B are summarized in Figure 28 and Tables 5 and 6. The cross-sectional areas and aspect ratios are calculated by approximating the microfeature as a rectangle.

Table 5. Feature Dimensions of Layout A electroplated for 48 hrs. Average dimensions are presented along with standard deviations and sample size.

Segment #	Height (um)	N	Width (um)	N	Cross-Sectional Area (mm^2)	Aspect Ratio (W/H)
1	209.55 ± 44.9	2	352.87 ± 47.9	2	0.0739	1.68
2	125.73 ± 10.7	4	245.14 ± 25.0	4	0.0308	1.95
3	76.20 ± 3.2	6	167.40 ± 9.7	6	0.0128	2.20
4	60.96 ± 4.4	3	113.93 ± 14.5	6	0.0069	1.87

Table 6. Feature Dimensions of Layout B electroplated for 72 hrs.

Segment #	Height (um)	N	Width (um)	N	Cross-Sec Area (mm^2)	Aspect Ratio (W/H)
1	226.06 ± 28.7	2	407.43 ± 17.5	2	0.0921	1.80
2	142.88 ± 12.5	4	286.74 ± 13.3	4	0.0410	2.01
3	76.41 ± 7.6	6	170.71 ± 20.3	8	0.0130	2.23
4	43.18 ± 14.1	3	80.75 ± 13.3	10	0.0033	1.75

There were significant variations in the feature sizes depending upon the layout and the time allowed for electrodeposition. Varying these parameters led to a wide range of potential cross-sectional areas. One unifying characteristic across all layouts, however, was the uniform aspect ratio of approximately two.

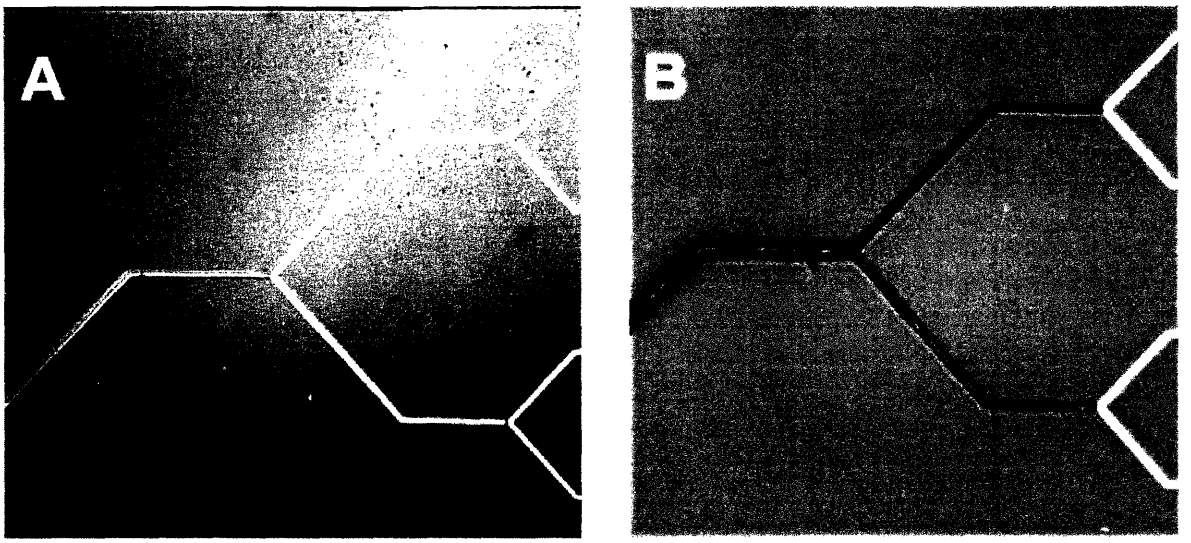

Figure 27. Electrodepostion of Nickel onto Patterned Conductive Gold Islands. A) Nickel is plating the first and second conductive islands several after initiation of electrodeposition. B) Several hours later, electrodeposition of nickel on the third segment commences.

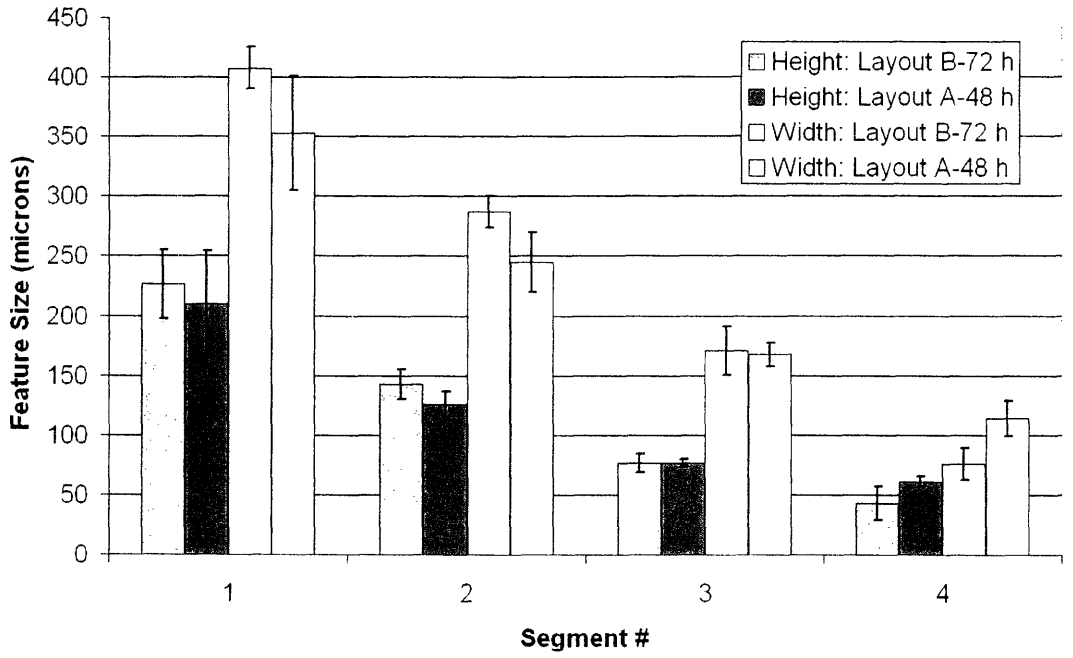

Figure 28. Microchannel Dimensions of Electrodeposited Nickel Masters (Layout A, 48 hrs of electrodeposition. Layout B, 72 hrs of electrodeposition). Both the feature height and width of the channels can be controlled as the cross-sectional areas of the microchannels are reduced. The gap distances are used to control the sharpness of the decrease in feature height and width while the final feature height can be controlled by the total time allowed for electrodeposition. The error bars represent standard deviations of sample measurements.

4.3.2 Ultra-thin Layers of PGS and Thin Walled PGS Scaffolds

The resulting thicknesses of spin coated PGS for selected recipes are shown in Figure 29. Thin PGS layers were then used as the unpatterned layer in the fabrication of PGS-based microfluidic scaffolds. An SEM cross-section of a microchannel is shown in Figure 30. The top layer of PGS measures approximately 24 microns in thickness while the height and width of the microchannel at the most narrow point are both approximately 20 microns.

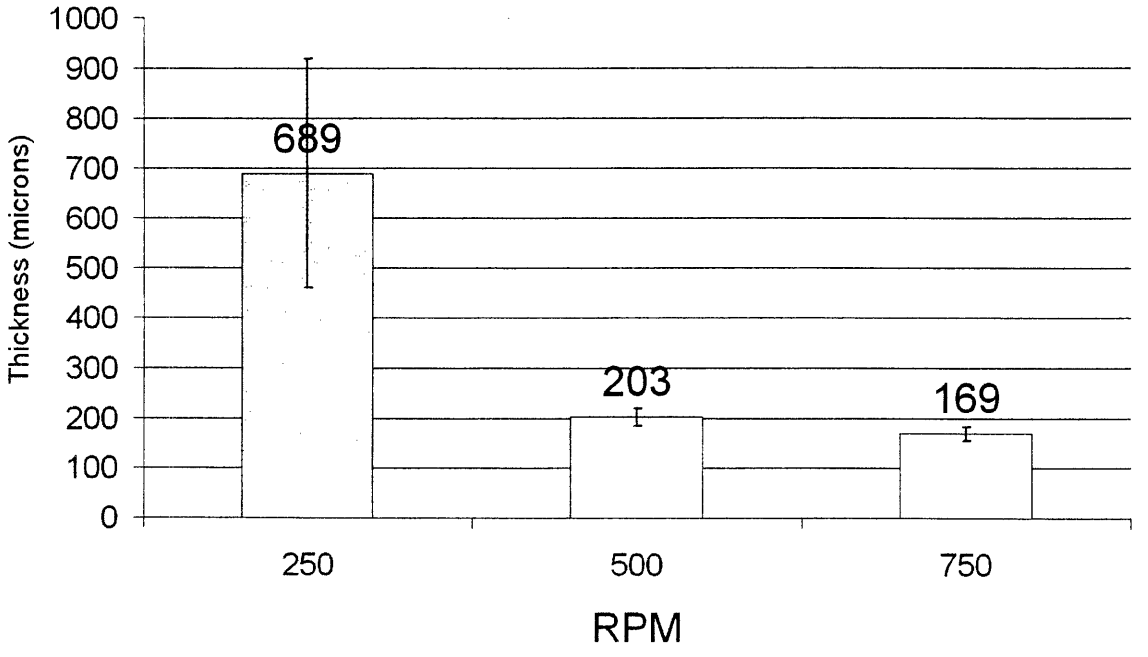

Figure 29. Thicknesses of Spin Coated PGS Membranes. Melted PGS pre-polymer can be spin coated onto various substrates to obtain very thin films. The film thicknesses obtained in this study were produced by melting the PGS to 120°C and spin coating at various speeds for 30 sec. The films were then cured using previously outlined methods (See Section 2.2.2). Error bars represent standard deviations of sample measurements across nine measurements.

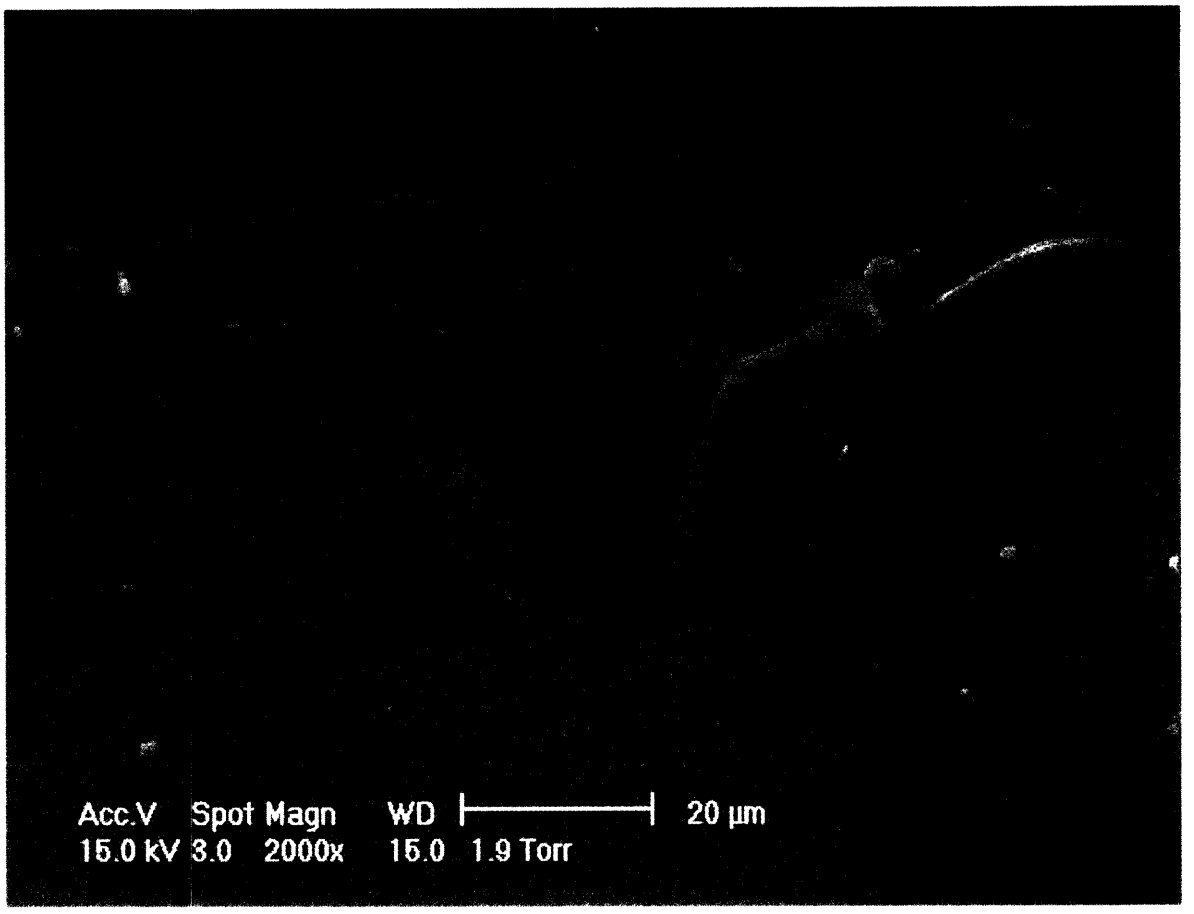

Figure 30. SEM Cross-section of a Thin-Walled PGS microchannel. This cross-section illustrates the structure of the microfluidic device that is fabricated by the protocol shown in Figure 26. While the thickness of the top layer of PGS is approximately 20 microns in this device, it can be adjusted by altering the PGS spin coating recipe.

4.4 Discussion

Standard microfluidic fabrication methods are used in a variety of applications including molecular and cell-based assays. Microfluidic systems have more recently been utilized as a method of efficiently controlling the cellular microenvironment. Subsequent studies have focused on monitoring the response of cells to a variety of microenvironment signals such as chemical gradients[61] and fluid shear stress[62]. Systems and devices used in primarily diagnostic or basic science studies do not require complex flow geometries or unique fabrication methods. However, directly

applying these existing fabrication techniques towards the production of microfluidic tissue engineering scaffolds is inadequate. One essential ideology for designing effective tissue engineering scaffolds is biomimicry in as many aspects as possible. In the specific case of vascular tissue engineering, special attention must be given in designing the micromechanical environment and the subsequent flow geometries within the scaffold. Furthermore, the dimensions of the device must allow sufficient mass transport to efficiently supply oxygen and nutrients. Traditional methods such as replica molding techniques of PDMS on a uniformed etched silicon master are not desirable for fabricating novel microfluidic tissue engineering scaffolds. This study investigated the potential for applying a method of cascading electrodeposition of conductive materials to fabricate multileveled structures. It has proven to be a useful technique to create multi-level metal structures in the world of microscale tissue engineering as well as MEMS in general.

4.4.1 Improved Channel Geometry

Fabricating channels that maintain a relatively constant aspect ratio of approximately unity would be ideal in the design of a biomimetic microfluidic device. The most critical design element in fabricating these scaffolds is the gap distance between the conductive islands. The lengths of these gaps directly impact the relative heights of each feature as well as the differential feature sizes from segment to segment. The final dimensions of the features are directly governed by the time allowed for electrodeposition. From the results plotted in Figure 28, it is clear that features with a wide range of cross-sectional areas and approximately constant aspect ratios can be obtained on the same device. Furthermore, if the gap distances are relatively large, then the size of the features decreases more rapidly from segment to segment. This result is intuitively obvious from Eqns. 4.1 and 4.2. The aspect ratios of silicon etched microfluidic masters (See Section 3.2.1) have a wide range of aspect ratios as the cross-sectional area is reduced. The aspect ratios of the electrodeposited nickel

remain approximately constant at a value of two. The potential for improvement in aspect ratios in channels is self-evident (Figure 31).

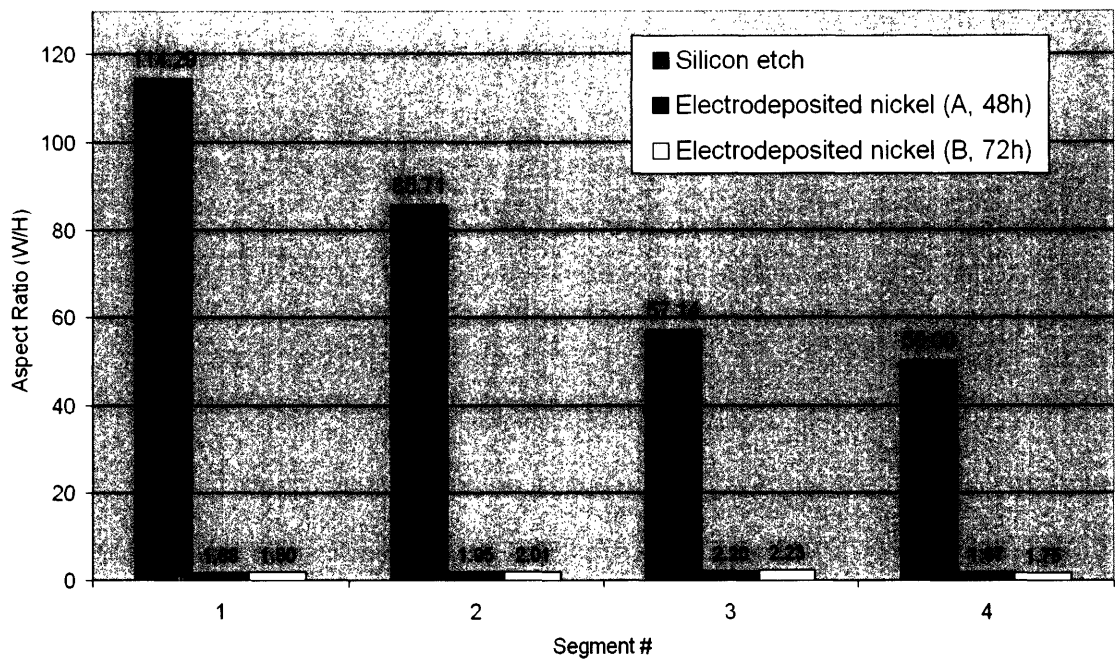

Figure 31. Improved Aspect Ratio of Microchannels of Electrodeposited Nickel Masters (Layout A, 48 hrs and Layout B, 72 hrs) vs. Silicon Etched.

Silicon masters traditionally used in microfluidics are etched to a constant depth with a variable channel width. This leads to oblong channel geometries and very large width-to-height aspect ratios. Multi-level nickel-based electrodeposition molds are able to maintain relatively constant aspect ratios of two. This improved channel geometry can result in improved fluid flow that more accurately mimics physiological microcirculation.

The slight variation in the aspect ratio for the electrodeposited nickel mold can be attributed to the increased effect of the initial width of the conductive island. The 25 micron initial width has a more significant effect on the aspect ratio of features that have smaller heights. Also, the deviations of the aspect ratios can also be attributed to variations in the electrodeposition across patterns. For

example, the conductive islands of the substrate that were located near the air-liquid interface of the electroplating bath plated more rapidly than other regions that were located deeper in the bath. In the plating of Layout A, the feature height of segments 3 and 4 could vary as much as 8 microns across segments from top to bottom across the device. These variations could be attributed to a variety of factors including chemical gradients, temperature gradients, non-uniform electric fields, and misalignment of the counter electrode.

4.4.2 Comparison to Existing Methods

Microfluidic devices with multiple channel heights has been previously studied through the use of multiple silicon etch processes on a single substrate. Consider the fabrication of a microfluidic master with three specified microchannel heights. This process flow requires three mask layouts and three etch processes. Consequently, there would have be multiple stages of photoresist patterning and silicon etching. The feature geometries would also exhibit salient edges throughout the layout. The regions of microfluidic reductions would also feature sharp, step changes in feature height. The electrodeposited method exhibits numerous advantages over a multiple etch process in terms of improved process efficiency and more accurate biomimicry. Microfabrication processes are both expensive and time-consuming. Therefore, the electrodeposition method reduces the time and resources required by requiring only one simple lift-off process as opposed to multiple steps of photoresist patterning, etching, and cleaning. Furthermore, electrodeposited multi-level molds exhibit improved geometry. The electrodeposited nickel structures have rounded geometries at the extents of features and across reductions in the cross-sectional area of the channels. Subsequent replica molding of microfluidic devices results in a smoother microfluidic channel.

4.4.3 Thin-Walled PGS Microfluidic Devices

The fabricated thin walled PGS scaffolds satisfy the design rules regarding oxygen supply outlined in Section 2.4.4. However, as previously mentioned, it is also beneficial to establish a system that supports convective transport across the microfluidic layers in the case of a stacked, multi-layered system. The technique for fabrication of thin-walled PGS-based microfluidic devices is also applicable to fabricating a wide range of modified devices that can be used in more complex systems. Salt particles could be incorporated into pre-polymer during the deposition of the unpatterned PGS layer. After bonding with the patterned layer, the salt particles could be dissolved in water to make a microfluidic devices with a porous layer. The unpatterned PGS layer could also be distributed on a substrate with various microstructures. Regularly spaced microposts could be used to fabricate PGS devices with vertical microchannels to allow convection between the microfluidic layers. A modified microfluidic system with vertical channels could be used in a perfusion co-culture system in combination with a porous scaffold. Endothelial cells could be cultured in the microfluidic device while hepatocytes could be cultured simultaneously in a porous PGS scaffold.

4.4.4 Summary and Future Work

The fabrication of microfluidic masters with multiple feature heights has been demonstrated. The flow patterns of said masters mainly consist of simple bifurcations with arbitrary scaling formulas. Therefore, these specific microfluidic devices have not been tailored to specific vascular tissue engineering applications. Second generation masters should be fabricated with more intricate designs in order to increase capillary density and obtain biomimetic flow geometries. Fabricating more complex devices requires increased accuracy during the electrodeposition process. The use of finite-element electrodynamic simulations could be useful in the assessment of non-uniform current

densities and voltage drops across conducting segments. Incorporation of information from these simulations could then be used in the design of more intricate layouts.

Conclusions

This work has developed materials and methods that represent significant improvements to existing microfluidic vascular tissue engineering strategies. Previous efforts have focused on directly applying standardized microfluidic materials and processes towards solving problems in tissue engineering. The first generation of microfluidic scaffolds used PDMS to fabricate relatively simple bioreactors for use in perfusion cell culture systems. Next generation systems, described in this thesis work, have focused on the integration of novel biodegradable materials in the fabrications of complex devices that are designed specifically with vascular tissue engineering applications in mind.

Permeability of poly(glycerol-sebacate). The use of poly(glycerol-sebacate) (PGS), a biodegradable elastomer with superior mechanical properties, will usher in a new generation of microfluidic devices and tissue engineering scaffolds in general. The permeability of solid PGS membranes to oxygen and carbon dioxide was initially measured using a simple time-lag diffusion experiment. These data were then incorporated into a simple diffusion-reaction model to determine the characteristic length scale for gas diffusion in solid PGS tissue engineering scaffolds. It was determined that cells seeded in PGS-based tissue engineering systems and constructs with large volumes will be susceptible to hypoxia.

Biodegradable Microfluidic Scaffolds for Endothelial Cell Culture. The presented work has also developed a baseline strategy for the fabrication of simple structures, devices, and systems using PGS. Special focus was given to the fabrication of microfluidic scaffolds. More specifically, methods for PGS replica molding and bonding of PGS sheets were successfully developed. However, there are numerous systems and devices with various forms and geometries that could be fabricated with the generalized techniques developed in this work. Long-term perfusion cell culture of human umbilical vascular endothelial cells was demonstrated in microfabricated PGS devices.

Complex Biodegradable Microfluidic Device Fabrication. More complex systems and fabrication methods have also been developed with PGS. These techniques are designed to produce devices that are specifically tailored to developing large-scale vascular tissue engineering scaffolds. PGS-based microfluidic scaffolds with layers of approximately 20 microns in thickness were fabricated to accommodate mass transfer limitations of oxygen and carbon dioxide. Microfluidic masters with biomimetic microchannel geometries were also fabricated using a novel three-dimensional electroplating technique. Uniform aspect ratios of the microchannels throughout the device were obtained.

Future Direction. This work has primarily focused on the application of PGS toward the fabrication of single-layered microfluidic tissue engineering scaffolds. PGS is a promising material for tissue engineering applications. Future work should focus on the scale-up of this existing technology to fabricate larger scaffolds using PGS. For example, multiple layers can be stacked, bonded, and interconnected to create three-dimensional scaffolds. Integrating multiple microfluidic systems with other materials to form composite scaffolds is also a promising new direction for organ regeneration. Complex organs contain many types of functional and supporting cells. Therefore, an ideal scaffold should be able to promote the proliferation and integration of these various cell types. PGS is a material that can be modified structurally and chemically. For example, RGD peptide sequences can be integrated into the nucleophillic polyester bonds in PGS. The degradation rate and hydrophobicity of the polymer can be modified by altering the stoichiometry of the monomers. Mircopatterning of specific PGS formulations in the form of foams or sheets could produce a scaffold with physical and chemical cues for the controlled proliferation and organization of various cells types. These scaffolds could be sandwiched between pre-existing vascularized microfluidic PGS layers. In addition to achieving sufficient supply of nutrients, the major issues to be addressed in developing tissue-engineering systems of this complexity are the spatial segregation of scaffold

properties and the fluidic connections within the scaffold. If these challenges are indeed met, then the co-culture of functional and supporting cells in a three-dimensional, vascularized, biodegradable scaffold is a significant and dramatic step toward the regeneration of functional organs and tissues.

References

1. Procedure Number: National Inpatient Profile 1991 Data, H.D.S.L.O.S.D.R.G., Federal Register, Department of Health and Human Services (Medicare-Based Information).
2. Data Derived from American Heart Association, A.D.A., American Liver Foundation, American Lung Foundation, American Kidney Foundation, Muscular Dystrophy Association, Industry Sources, Et. Al. (2003).
3. Kusama K., D.W.I., Samter G., *Dis. Colon Rectum* **32**, 694 (1989).
4. www.Donatelifeny.Org Organ Donor Statistics. (2003).
5. Langer R. S., V.J.P. Tissue Engineering. *Science* **260**, 920-926 (1993).
6. Ross R. *Nature*, 801 (1993).
7. Duffy D. C., M.J.C., Schueller J. A., Whitesides G. M. Rapid Prototyping of Microfluidic Systems in Poly(Dimethylsiloxane). *Analytical Chemistry* **70**, 4974-4984 (1998).
8. Ramsauer M., D.A.P.A. *J. Clin. Invest.* **110**, 1615-1617 (2002).
9. Jain R. K. Molecular Regulation of Vessel Maturation. *Nature Medicine* **9**, 685-693 (2003).
10. Hellstrom M., E.A. Role of Pdgf-B and Pdgfr-B in Recruitment of Vascular Smooth Muscle Cells and Pericytes During Embryonic Blood Vessel Formation in the Mouse. *Development* **126**, 3047-3055 (1999).
11. D'amore P. Angiogenesis Biochemistry Overview.
12. Rudolfsson S. H., J.A., Et. Al. Localized Expression of Angiopoietin 1 and 2 May Explain Unique Characteristics of the Rat Testicular Microvasculature. *Biology of Reproduction* **69**, 1231-1237 (2003).
13. Cleaver O., M.D.A. Endothelial Signaling During Development. *Nature Medicine* **19**, 661-668 (2003).
14. Egginton S., E.A. Unorthodox Angiogenesis in Skeletal Muscle. *Cardiovasc. Res.* **49**, 643-646.
15. Resnick N., Y.H., Shay-Salit A., Shushy M., Schubert S., Zilberman L., Wofovitz E., Fluid Shear Stress and the Vascular Endothelium: For Better and for Worse. *Progress in Biophysics and Molecular Biology* **81**, 177-199 (2003).
16. Hsieh H. J., E.A. Pulsatile and Steady Flow Induces C-Fos Expression in Human Endothelial Cells. *J. Cell. Physiol.* **154**, 143-151.
17. Ando J., E.A. Shear Stress Inhibits Adhesion of Culture Mouse Endothelial Cells to Lymphocytes by Downregulating Vcam-1 Expression. *American Journal of Physiology* **267**, C679-697.
18. Thompson C. A., E.A. A Novel Pulsatile, Laminar Flow Bioreactor for the Development of Tissue-Engineered Vascular Structures. *Tissue Eng.* **8**, 1083-1088 (2002).
19. Bettinger C. J. CFD of Capillary Networks. (2003).
20. Semenza G. L. O2-Regulated Gene Expression: Transcriptional Control of Cardiorespiratory Physiology by Hif-1. *Journal of Applied Physiology* **96**, 1173-1177 (2004).
21. Xu L., F.D., Jain R. K., Acidic Extracellular Ph Induces Vascular Endothelial Growth Factor (Vegf) in Human Glioblastoma Cells Via Erk1/2 Mapk Signaling Pathway: Mechanism of Low Ph-Induced Vegf. *J. of Biol. Chem.* **277**, 11368-11374 (2002).
22. Lee K. Y., P.M.C., Anderson K. W., Mooney D. J. Controlled Growth Factor Release from Synthetic Extracellular Matrices. *Nature* **408**, 998-1000 (2000).
23. Richardson D. M., P.M.C., Ennet A. B., Mooney D. J., *Nature Biotechnology* **19**, 1029-1034 (2001).

24. Herttuala S. Y., A.K. Gene Transfer as a Tool to Induce Therapeutic Vascular Growth. *Nature Medicine* **9**, 694-701 (2003).
25. Levenberg S., G.J.S., Amit M., Itskovitz-Eldor J., Langer R., Endothelial Cells Derived from Human Embryonic Stem Cells. *Proc. Natl. Acad. Sci. U.S.A* **99**, 4391-4396 (2002).
26. Levenberg S., H.N.F., Lavik E., Rogers A. B., Itskovitz-Eldor J., Langer R., Differentiation of Human Embryonic Stem Cells on Three-Dimensional Polymer Scaffolds. *Proc. Natl. Acad. Sci. U.S.A* **100**, 12741-12746 (2003).
27. Nikalson L E, G.J., Abbott W M, Hirschi K K, Houser S, Marini R, Langer, R Functional Arteries Grown in Vitro. *Science* **284**, 489-493 (1999).
28. Kaihara S., B.J., Koka R., Lalan S., Ochoa E. R., Ravens M., Pien H., Cunningham B., Vacanti J. P. Silicon Micromachining to Tissue Engineer Branched Vascular Channels for Liver Fabrication. *Tissue Engineering* **6**, 105-117 (2000).
29. Chiu D.T., J.N.L., Huang S., Kane R.S., Wargo C.J. Choi I.S., Ingber D. E., Whitesides G.M., *Proc. Natl. Acad. Sci. U.S.A* **12**, 2408-2413 (2000).
30. Borenstein J. T., T.H., King K. R., Weinberg E. J., Kaazempur-Mofrad M. R., Vacanti J. P. Microfabrication Technology for Vascularized Tissue Engineering. *Biomedical Microdevices* **4**, 167-175 (2002).
31. King K. R., W.C., Vacanti J. P., Borenstein J. T., Biodegradable Polymer Microfluidics for Tissue Engineering Microvasculature. *Materials Research Society Symposium Proceedings - BioMEMS and Bionanotechnology* (2002).
32. Leclerc E., Y.S., Fujii T., Cell Culture in 3-Dimensional Microfluidic Structure of Pdms (Polydimethylsiloxane). *Biomedical Microdevices* **5**, 109-114 (2003).
33. Tan W., D.T.A. Layer-by-Layer Microfluidics for Biomimetic Three-Dimensional Structures. *Biomaterials* **24**, 1355-1364 (2004).
34. Langer R., P.N.A. New Challenges in Biomaterials. *Science* **263**, 1715-1720 (1994).
35. Yannas I. V., B.J.F., Orgill D. P., Skrabut E. M., Wound Tissue Can Utilize a Polymeric Template to Synthesize a Functional Extension of the Skin. *Science* **215**, 174 (1982).
36. Hubbell J., L.R. Tissue Engineering. *Chemical and Engineering News* **42** (1995).
37. Langer R. Biomaterials: Status, Challenges, and Perspectives. *AIChE J.* **46**, 1286-1289.
38. Mikos A., B.Y., Ingber D., Vacanti J., Langer R., Preparation of Poly(Glycolic Acid) Bonded Fiber Structures for Cell Transplantation. *Journal of Biomedical Materials Research* **27**, 183 (1993).
39. Lee K. Y., E.A. Controlling Mechanical and Swelling Properties of Alginate Hydrogels Independently by Cross-Linker Type and Cross-Linking Density. *Macromolecules* **33**, 4291-4294 (2000).
40. Urry, D.W., Et. Al. *J. Biomaterials Science, Polymer Edition* **9** (1998).
41. Van Hest, J.C.M., Tirrell, D.A., Protein-Based Materials, toward a New Level of Structural Control. *Chem. Comm.* **19**, 1897-1904 (2001).
42. Welsh, E.R. *Biomacromolecules* **1**, 23-30 (2000).
43. Sodian, R., Et. Al. *Tissue Eng.* **6**, 183-187 (2000).
44. Langer R., P.N.A. Advances in Biomaterials, Drug Delivery, and Bionanotechnology. *AIChE Journal* **49**, 2990-3006 (2003).
45. Qiu Y, P.K. Superporous Ipn Hydrogels Having Enhanced Mechanical Properties. *AAPS PharmSciTech* **4** (2003).
46. Madison L. L., H.G.W. Metabolic Engineering of Poly(3-Hydroxyalkanoates): From DNA to Plastic. *Microbiology and Molecular Biology Reviews* **63**, 21-53 (1999).
47. Williams S.F., M.D.P. Applications of Phas in Medicine and Pharmacy. (1999).

48. Wang Y., K.Y.M., Langer R., In Vivo Degradation Characteristics of Poly(Glycerol-Sebacate). *Journal of Biomedical Materials Research* **66A**, 192-197 (2003).
49. Wang Y., A.G.A., Sheppard B. J., Langer R. A Tough Biodegradable Elastomer. *Nature Biotechnology* **20**, 602-606 (2002).
50. Sok R. M. Permeation of Small Molecules across a Polymer Membrane: A Computer Simulation Study. *University Library Groningen* **Dissertation**, 1-129 (1994).
51. Graham T. Solution-Diffusion Mechanism for Gases in Polymers. *Philos. Mag.* **32**, 401 (1866).
52. Daynes H. A. Time-Lag Gas Permeability Measurements in Polymers. *Proc. Roy. Soc. Lond, Series A* **97**, 286 (1920).
53. Mulder M. Basic Principles of Membrane Technology, Edn. 2nd. (Kluwer Academic Publishers, Boston; 1996).
54. Odian G. Principles of Polymerization, Edn. 3rd. (Wiley-Interscience, New York; 1991).
55. Thomson R.C., Y.R.M., Mikos A.G., Principles of Tissue Engineering. (Landes & Co., 1997).
56. Vacanti J.P., L.R. Supplement 1. *Lancet* **354** (1999).
57. Lavan D., G.P.M., Langer R. Simple, Three-Dimensional Microfabrication of Electrodeposited Structures. *Angewandte Chemie* **42**, 1262-1265 (2003).
58. www.Mems-Exchange.Com Gold Lift-Off I. (2004).
59. Safranek W.H. The Properties of Electrodeposited Metals and Alloys: A Handbook, 2nd Ed. (American Electroplaters and Surface Finishers Society, Orlando, FL; 1986).
60. Buchheit T.E., L.D.A., Micael J.R., Christenson T.R., Leith S.D., *Metall. Mater. Trans. A* **33**, 539 (2002).
61. Jeon N. L., B.H., Dertinger S. K. W., Whitesides G. M., Livingston V. W., Toner M., Neutrophil Chemotaxis in Linear and Complex Gradients of Interleukin-8 Formed in a Microfabricated Device. *Nature Biotechnology* **20**, 826-830 (2002).
62. Wang J. H., G.-C.P., Wille J., Yin F. C., Specificity of Endothelial Cell Reorientation in Response to Cyclic Mechanical Stretching. *Journal of Biomechanics* **34**, 1563-1572 (2001).

[This Page Intentionally Left Blank]

[This Page Intentionally Left Blank]

[This Page Intentionally Left Blank]